Tellus METEOROLOGY
PUBLISHED BY THE INTERNATIONAL METEOROLOGICAL INSTITUTE IN STOCKHOLM

Identifying sensitivities for cirrus modelling using a two-moment two-mode bulk microphysics scheme

By CARMEN G. KÖHLER[1,3]* and AXEL SEIFERT[2], [1]*Deutscher Wetterdienst, Offenbach, Germany;* [2]*Hans-Ertel Centre for Weather Research, Deutscher Wetterdienst, Hamburg, Germany;* [3]*Deutsches Zentrum für Luft- & Raumfahrt, Institut für Physik der Atmosphäre, Oberpfaffenhofen, Germany*

(Manuscript received 31 March 2014; in final form 7 December 2014)

ABSTRACT

Cirrus cloud genesis is an inherently multiscale and non-linear problem. The synoptic scale provides the environment, the mesoscale determines the forcing and the actual nucleation events occur on a microscopic scale. This makes the parameterisation in numerical weather prediction models a challenging task. In order to improve the prediction of cirrus clouds and ice supersaturation formation in the German Weather Service (DWD) model chain, the controlling physical processes are investigated and parameterised in a new cloud ice microphysics scheme. The new scheme is an extended version of the ice-microphysical scheme operational in the numerical weather prediction models of DWD. The developed two-moment two-mode cloud ice scheme includes state-of-the-art parameterisations for the two main processes for ice formation, namely homogeneous and heterogeneous nucleation. Homogeneous freezing of supercooled liquid aerosols is triggered in regions with high atmospheric ice supersaturations (145–160%) and high cooling rates. Atmospheric small-scale fluctuations are accounted for by use of the turbulent kinetic energy. Heterogeneous nucleation depends mostly on the existence of ice nuclei in the atmosphere and occurs primarily at lower ice supersaturations. Thus, heterogeneously nucleated ice crystals deplete ice supersaturation via depositional growth and can therefore inhibit subsequent homogeneous freezing. The new cloud ice scheme accounts for pre-existing ice crystals, contains a prognostic budget variable for activated ice nuclei and includes cloud ice sedimentation. Furthermore, a consistent treatment of the depositional growth of the two-ice particle modes and the larger snowflakes is applied by using a relaxation time scale method which ensures a physical representation for depleting ice supersaturation. The new cloud ice scheme is used to identify the relative roles of heterogeneous and homogeneous nucleation in the formation of cirrus clouds and ice supersaturation. A parcel model is used in order to investigate the differences between the operational and new cloud ice scheme. The time scales for the homogeneous nucleation event and for the depositional growth are emphasised. The importance of the new ice nucleation scheme is demonstrated by conducting idealised simulations of orographic cirrus in the COSMO (Consortium for Small-Scale Modeling) model environment.

Keywords: cloud microphysics, ice nucleation, cirrus clouds, ice supersaturation

1. Introduction

Cirrus clouds significantly influence the radiative properties of the atmosphere and have a high impact on climate and weather (Liou, 1986). Consequently, cirrus cloud parameterisations used in numerical weather prediction (NWP) models have been a target of growing attention. Through high performance computing and higher grid resolutions, important processes can be explicitly modelled and less limiting assumptions are needed. These improvements lead to the possibility to represent the microphysical processes in a more complete and sophisticated way in NWP models.

Anthropogenic effects on climate are increasing in importance, for example, through the impact of airplanes on climate change. When airplanes fly through regions with ice supersaturated air, climate-impacting condensation trails (contrails) can form (Schumann, 2002). Soot from the aircraft emissions is thought to be the dominant aerosol for contrail formation (Heymsfield et al., 2010). Contrails can also form in already existing cirrus clouds, making the previously formed cirrus more opaque. The influence of

*Corresponding author.
email: carmen.koehler@dwd.de
Responsible Editor: Annica Ekman, Stockholm University, Sweden.

Citation: Tellus B 2015, **67**, 24494, http://dx.doi.org/10.3402/tellusb.v67.24494

contrails and contrail-induced cloudiness is of particular interest for climate studies (Burkhardt and Kärcher, 2011). The possibility of a correct ice supersaturation forecast yields the potential to predict the formation of aircraft induced contrail cirrus (Mannstein, 2008). Thus, it is of interest to localise the regions of ice supersaturation occurrence in order to conduct flight level changes to reduce anthropogenic cloudiness. For predicting ice supersaturated regions, a physically based representation of cirrus and ice supersaturation in NWP models is desirable. Especially the process of depositional growth of ice crystals has a substantial influence on the depletion of ice supersaturation.

The main mechanisms for cirrus formation are (1) homogeneous and (2) heterogeneous freezing. (1) Homogeneous freezing of pure cloud droplets occurs at approximately -38°C (Heymsfield and Sabin, 1989), but aqueous solutions of droplets freeze homogeneously at temperatures colder than -38°C. This takes place in regions of strong vertical updrafts and, in addition to sufficiently low temperature, substantial ice supersaturation is necessary with typical values ranging between 140 and 180% (Krämer et al., 2009). Homogeneous nucleation of supercooled liquid aerosol particles results in small ice crystal particles with a high number density of $n_i = 0.1$–50 cm^{-3} due to atmospheric small-scale temperature fluctuations (Hoyle et al., 2005). (2) Heterogeneous freezing causes the ice crystal particles to be of greater size but of a lower number density than homogeneously nucleated ice crystals (DeMott et al., 1997). Heterogeneous ice requires the presence of ice nuclei (IN) and can already occur at relatively low ice supersaturations compared to homogeneous nucleation. Consequently, depending on the ambient atmosphere, different nucleation regimes determine cirrus cloud formation, which complicates the parameterisation and numerical implementation of these processes in atmospheric models.

Compared to homogeneous nucleation, there are still a lot of uncertainties concerning heterogeneous nucleation and the nucleation characteristics for each IN species (DeMott et al., 2011). The ongoing debate concerning the influence of IN on cirrus clouds was also addressed in the latest IPCC Report (Boucher et al., 2013). An additional challenge for cirrus modelling is posed by the lack of understanding of the respective roles of homogeneous and heterogeneous nucleation for different ambient conditions (Baumgardner et al., 2012). Results from the 'Cirrus Parcel Model Comparison Project' (Lin et al., 2002) suggest the critical components in cirrus modelling to be the homogeneous nucleation rate and the depositional growth of ice crystals. In particular, the depositional coefficient α_d causes the simulations of the depositional growth rate to deviate, as α_d controls the water vapour uptake rate. These issues are discussed in the following and sensitivities for cirrus cloud modelling are elucidated.

For example, Morrison et al. (2005a) and Spichtinger and Gierens (2009a) belong to studies describing double-moment bulk microphysics schemes which describe cirrus formation and account for the two main processes, homogeneous and heterogeneous nucleation. In this study, for a more detailed representation and understanding of the ice nucleation processes, the ice crystals are divided into two different modes originating from homogeneous and heterogeneous nucleation, respectively. Prognostic variables for the number densities are implemented in addition to the mass mixing cloud ice ratios, leading to a two-moment two-mode cloud ice scheme. The microphysics scheme of the operational COSMO (Consortium for Small-Scale Modeling) model (Doms et al., 2007) is extended with a more sophisticated parameterisation for homogeneous and heterogeneous freezing. For homogeneous freezing of liquid aerosols, the scheme proposed in Kärcher et al. (2006) was chosen as it includes the competition of both nucleation processes by accounting for pre-existing ice. The operational heterogeneous nucleation scheme, a modified version of Fletcher (1962), was replaced by the scheme of Phillips et al. (2008), which includes three classes of aerosols, with the possibility of being coupled to a model aerosol climatology or chemistry models. In this study however, the initial aerosol number concentrations suggested in Phillips et al. (2008) are used. In order to prevent an overestimation as a result of too many available IN, the new cloud ice scheme includes a budget variable to track previously activated aerosol particles. Also, the cloud ice sedimentation scheme proposed in Khvorostyanov and Curry (2005) is implemented. The new cloud ice scheme also contains a physically based deposition/sublimation formulation, where a relaxation time scale approach of the two small-particle cloud ice modes and the larger snowflakes is applied, following Morrison et al. (2005a).

First, the ice nucleation parameterisations are introduced using a parcel model. These are outlined whilst the changes made for the two-moment two-mode scheme are explained. Varying the initial aerosol number densities and the forcing resulting from different mountain heights, a parameter study with idealised simulations of orographic clouds in the COSMO model environment is conducted. The successive introduction of the budget variable for IN tracking, and the cloud ice sedimentation shows direct effects on the interaction between homogeneous and heterogeneous nucleation.

2. Parcel model framework

The two-moment two-mode cloud ice scheme is implemented in a parcel model in order to investigate the effects and sensitivities of the different nucleation mechanisms.

The parcel model study serves as a documentation of the new cloud ice scheme. The documented changes include the description of the parameterisations for the heterogeneous and homogeneous nucleation. The depositional growth of ice crystals and its role in the depletion of ice supersaturation are also explained. Afterwards, the entire cloud ice scheme is tested in the parcel model environment, where the emphasis lies on the interaction of both nucleation mechanisms. The simple framework serves as a tool to compare the ice nucleation schemes of the operational COSMO model to the newly implemented cloud ice scheme in a straightforward manner. Further parcel model studies for ice nucleation are, for example, Gierens (2003), Liu and Penner (2005), Kay et al. (2006), Barahona and Nenes (2008), Eidhammer et al. (2009) and Spichtinger and Gierens (2009a).

2.1. Parcel model setup

An air parcel is studied which is lifted dry adiabatically in upper-tropospheric conditions. Of interest are the ice saturation ratio S_i, the cloud ice mixing ratio q_i, the ice crystal number density n_i, the ice particle radius r_i and the resulting cloud ice mass m_i. The ice saturation ratio is defined as

$$S_i = \frac{e_v}{e_{si}(T)} \tag{1}$$

with e_v and e_{si} being the vapour pressure and the saturation vapour pressure over ice, respectively, where the latter is calculated following Murphy and Koop (2005). The air parcel rises with a constant velocity w where the adiabatic cooling causes the ice saturation ratio S_i to increase. Heterogeneous nucleation can occur at low ice supersaturations if IN are available. Homogeneous freezing can occur at substantially high ice supersaturations which are caused by high cooling rates, mixing or diabatic cooling (Spichtinger et al., 2005). Once ice crystals have formed, depositional growth decreases the water vapour mixing ratio q_v, thereby depleting the ice supersaturation.

The initial conditions used in the parcel model are specified by pressure p, temperature T, vertical velocity w and the ice saturation ratio S_i. Additional parameters are the time step Δt and the typical number density of liquid aerosol particles (1000 cm^{-3}) and background aerosol particles that potentially act as IN (1–30 dm^{-3}). A monodisperse distribution and an initial aerosol particle radius prior to freezing of $r_{i,0} = 0.25$ μm is assumed. The initial particles are considered spherical and thus the mass $m_{i,0}$ of the ice particles is calculated through

$$m_{i,0} = \frac{4\pi}{3}\rho_i r_{i,0}^3 \tag{2}$$

with the ice particle mass density $\rho_i = 0.925 \times 10^3$ kg m^{-3}.

The two-moment two-mode cloud ice variables are the ice crystal number densities $n_{i,hom}$ and $n_{i,het}$ with the ice mass mixing ratios $q_{i,hom}$ and $q_{i,het}$ for homogeneous and heterogeneous nucleation, respectively. The temporal evolution of the freezing process is described by a conservation equation for water mass and the temperature equation incorporates latent heat release and adiabatic cooling:

$$0 = \frac{dq_v}{dt} + \frac{dq_{i,hom}}{dt} + \frac{dq_{i,het}}{dt} \tag{3}$$

$$\frac{dT}{dt} = \frac{dq_v}{dt}\frac{L_s}{c_p} - \frac{g}{c_p}w \tag{4}$$

where $g = 9.81$ m s^{-2} is the acceleration by gravity and $c_p = 1005$ J kg^{-1} K^{-1} is the specific heat capacity of air at constant pressure. The equations are numerically integrated using the Euler forward scheme.

2.2. Parameterisation of heterogeneous nucleation

Heterogeneous nucleation occurs at temperatures above -40°C and depends on the existence of IN in the atmosphere. Parameterisations for heterogeneous nucleation have been suggested by, for example, Hoose et al. (2010) and Kärcher and Lohmann (2003). In the past, empirical parameterisations have been developed in which the IN depend on either ice supersaturation (e.g. Meyers et al., 1992), temperature, or both. The heterogeneous nucleation parameterisation scheme by Fletcher (1962), which is currently implemented in an altered form in the DWD models, is temperature dependent. In the following, the modified Fletcher parameterisation is compared to the heterogeneous ice nucleation scheme from Phillips et al. (2008; PDA08 hereafter).

In the operational models at the DWD, the empirical parameterisation of heterogeneous nucleation only depends on the temperature and does not differentiate between the different nucleation modes; that is, it summarises condensation, immersion, contact and deposition freezing in a single empirical equation. The classical Fletcher formula (Fletcher, 1962) is given by

$$n_{i,het} = n_0 \exp(0.6(T_0 - T)) \tag{5}$$

with $n_0 = 0.01$ m^{-3} and $T_0 = 273.15$ K. The ice crystal numbers resulting from eq. (5) at $T \approx -40$°C are found to overestimate $n_{i,het}$ by three orders of magnitude and underestimates the IN concentrations by about two orders of magnitude at moderately low temperatures $T \approx -10$°C (Doms et al., 2004). In order to counteract underestimations at high temperatures, additional so-called ice enhancement (e.g. ice crystal fragmentation, ice splinter production in riming) is implicitly taken into account.

The operational ice nucleation parameterisation for the number density of ice crystals results in

$$n_{\mathrm{i,het}}(T) = n_0 \exp(0.2(T_0 - T)) \tag{6}$$

and is based on a fit to aircraft measurements in stratiform clouds (Hobbs and Rangno, 1985; Meyers et al., 1992) where $n_0 = 100\ \mathrm{m}^{-3}$ is an empirical parameter (Doms et al., 2007). Comparisons of the activated IN n_{IN} resulting from eq. (6) and the PDA08 parameterisation are shown in Fig. 1a. This comparison shows that for low supercooling values $T < -20°\mathrm{C}$ the number of activated IN resulting from eq. (6) are significantly higher than those from the PDA08 scheme. Further comparisons of the resulting cloud ice number densities are illustrated and discussed in Section 2.5.

In the parameterisation proposed in PDA08, the number density of heterogeneous cloud ice is derived by using empirical dependencies of aerosol chemistry and accounting for various IN (see Appendix A.1). These are obtained by assuming the number of active IN to be approximately proportional to the aerosol's total surface area. The data used is constrained by measurements with a continuous flow diffusion chamber (CFDC). The PDA08 heterogeneous nucleation scheme explicitly distinguishes between inorganic black carbon (BC), insoluble organic carbon (O) and dust/metallic (DM) aerosols. The explicit handling of aerosol modes permits a future coupling to aerosol model climatologies. In this work, the initial number densities for the IN are set as proposed in PDA08, namely $n_{\mathrm{DM}} = 162\ \mathrm{dm}^{-3}$, $n_{\mathrm{BC}} = 15\ \mathrm{cm}^{-3}$ and $n_{\mathrm{O}} = 1.77\ \mathrm{cm}^{-3}$, which are based on six field campaigns. Sensitivity studies concerning these initial IN values and their influence in NWP models will be conducted in the idealised simulations in Section 4. The activated IN number densities, which result from the PDA08 scheme for the deposition and condensation/immersion modes in dependence of supersaturation over ice and supercooling, are depicted in Fig. 1, respectively. Comparisons presented in PDA08 show that the resulting number concentrations for heterogeneously nucleated ice crystals are in the same range as the Lohmann and Diehl (2006), Liu and Penner (2005), Khvorostyanov and Curry (2004) and Meyers et al. (1992) schemes. A validation and further discussions of this scheme can be found in Eidhammer et al. (2009) and Phillips et al. (2009). Phillips et al. (2013) suggest an improved approach of this heterogeneous nucleation scheme, but in this study the original PDA08 scheme is used. A comparison of the latter and the revised heterogeneous nucleation schemes with respect to soot can be found in Yun et al. (2013). Differences in soot properties and coating can strongly alter the ice nucleation abilities. The idea that soot is an important or even dominant IN is also questioned by recent studies, for example in Czizco et al. (2013). For our study, however, the attribution of IN to specific species is not important, as only the sum of the activated IN is considered and sensitivity studies are conducted for the total number of IN, but not for the individual aerosol species.

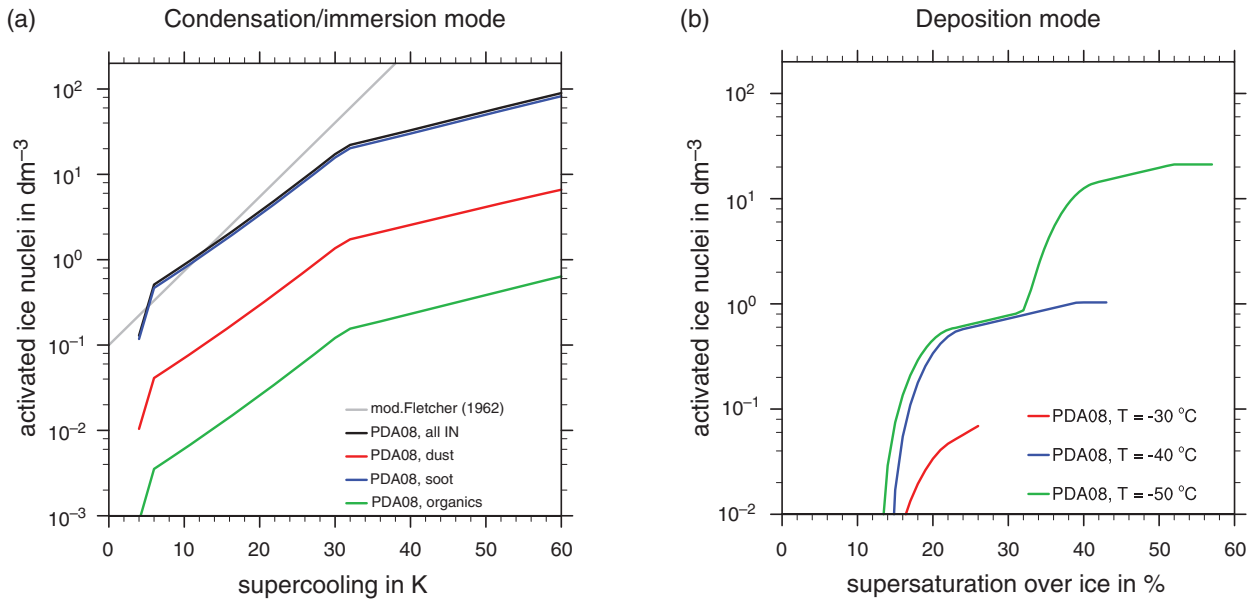

Fig. 1. The activated ice nuclei (IN) for soot, insoluble organic carbon and dust/metallic particles according to Phillips et al. (2008) using the initial number densities $n_{\mathrm{DM}} = 162\ \mathrm{dm}^{-3}$, $n_{\mathrm{BC}} = 15\ \mathrm{cm}^{-3}$ and $n_{\mathrm{O}} = 1.77\ \mathrm{cm}^{-3}$. The plots depict the activated IN for (a) the condensation/immersion freezing mode as a function of temperature assuming saturation w.r.t. liquid water and (b) the deposition mode as a function of supersaturation over ice and temperature (different colours). The activated IN number density from the modified Fletcher (1962) equation is depicted by the grey line, and the contribution from different aerosol species for PDA08 are shown with different colours.

2.3. *Parameterisation of homogeneous nucleation*

Homogeneous freezing of liquid aerosols is considered to be the dominant mode in cirrus formation below $-35°C$ (Sassen and Dodd, 1988). Yet, in the NWP models at the DWD, and most cloud resolving models, (see for example Thompson et al. (2004)) only homogeneous freezing of cloud water at temperatures below $-37°C$ is accounted for, while freezing of liquid aerosols is not yet included in the microphysical scheme. Various parameterisations for general circulation models exist [e.g. Barahona and Nenes (2008) and Kärcher and Burkhardt (2008)]. The homogeneous nucleation parameterisation of choice used in this work is based on Kärcher et al. (2006; KHL06 hereafter) with additional criteria for triggering the nucleation event. The KHL06 scheme is chosen as it includes the competition of both nucleation processes through accounting for pre-existing ice. Also, it is most appropriate for our application, that is, the range of scales we are targeting. The KHL06 homogeneous nucleation scheme also performs well in comparison with the reference scheme based on Koop et al. (2000).

As heterogeneous nucleation occurs at warmer temperatures, that is, $T > -40°C$, pre-existing heterogeneously formed ice crystals can reduce ice supersaturation before homogeneous freezing can set in. An overestimation of heterogeneously formed ice crystals by an ice nucleation scheme can lead to a suppression of homogeneous freezing. The pre-existing heterogeneously formed ice crystals deplete the existing ice supersaturation and thus prevent subsequent homogeneous nucleation. The KHL06 parameterisation accounts for the resulting competition between the homogeneous and the heterogeneous nucleation processes. This is done by using a fictitious vertical velocity w_p which accounts for pre-existing ice particles (see Appendix A.2.II). As lower velocities cause lower ice supersaturations, reducing the velocity has the same effect as nucleated crystals that deplete the saturation due to depositional growth. Following KHL06, homogeneous nucleation is only triggered if the model updraft w is larger than the fictitious vertical velocity w_p. Thus, in the case of $w < w_p$ any further nucleation is suppressed. The fictitious vertical velocity w_p and basic equations from the KHL06 scheme are given in Appendix A.2.II.

The challenge to correctly capture the homogeneous nucleation event in mesoscale models lies in the differing time scales. The time scales relevant for modelling the nucleation event consist of the model time step Δt, the point in time at which the homogeneous nucleation event commences t_{cr}, the duration of the freezing event τ_{freez} and the time period for the ice crystals to relax the ice supersaturation to a quasi-steady state, that is, the time scale for depositional growth τ_{dep}. These three time scales and t_{cr} are depicted in Fig. 2. For an upper-tropospheric temperature of $T = 220$ K and a vertical velocity of $w = 10$ cm s^{-1} typical values for the time scales are $\tau_{freez} = 20$ s and $\tau_{dep} = 2000$ s. The differing magnitudes of these time scales can present a potential difficulty for NWP models, in dependence of the length of their model time step. For process-oriented models the model time steps are only a few seconds, yielding the relations $\Delta t < \tau_{freez} < \tau_{dep}$. On the other hand climate models and some global models, for example, the Integrated Forecast System (IFS) of the European Center of Medium-range Forecast (ECMWF), typically have model time steps of several minutes and thus the time scale relations are $\tau_{freez} < \tau_{dep} < \Delta t$. For the DWD model chain this is more complex, as the scheme has to be valid for both regimes, that is, for the high-resolution regional COSMO model (Baldauf et al., 2011) with $\Delta t = 25$ s and for the global model GME (Majewski et al., 2002) with $\Delta t = 133$ s. The model time steps Δt are thus too large to fully resolve the freezing event but are too small to entirely include the freezing event as $\Delta t \approx \tau_{freez}$. The time scale relations consequently vary between $\Delta t < \tau_{freez} < \tau_{dep}$, $\tau_{freez} < \tau_{dep} < \Delta t$ and $\tau_{freez} < \Delta t < \tau_{dep}$, depending on the model.

In order to take these time scale differences into account, the onset and time interval of the nucleation event is determined. For this, the critical ice supersaturation ratio

$$S_{i,cr} = 2.349 - \frac{T}{259.00K} \tag{7}$$

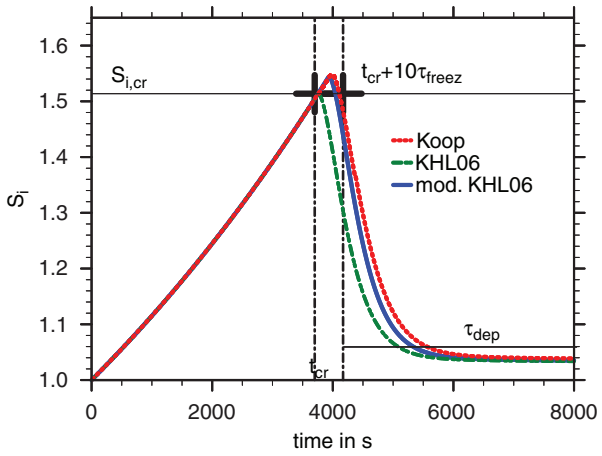

Fig. 2. The development of ice supersaturation over time of an adiabatically rising air parcel with the initial conditions $T = 220$ K, $p = 220$ hPa and a constant updraft $w = 10$ cm s^{-1}. The homogeneous nucleation scheme based on Koop et al. (2000) is compared to the KHL06 scheme and the KHL06 with a modified trigger mechanism. The nucleation event begins as soon as the critical ice supersaturation ratio $S_{i,cr}$ is reached at time t_{cr}. The duration of the nucleation event is denoted by $t_{cr} + 10\ \tau_{freez}$ and the depositional time scales is τ_{dep}.

is used as the threshold at which homogeneous nucleation is triggered. This threshold is a temperature dependent analytical fit from Ren and MacKenzie (2005) based on the results from Koop et al. (2000) and also used in KHL06. The time at which $S_{i,cr}$ is reached is calculated by

$$t_{cr} = \frac{1}{a_1 w} \ln\left(\frac{S_{i,cr}}{S_i}\right) \quad with \quad a_1 = \frac{L_s M_w g}{c_p R T^2} - \frac{Mg}{RT} \tag{8}$$

where L_s is the latent heat of sublimation, M_w the molecular mass of water, R the universal gas constant and M the molecular mass of air.

The characteristic time scale from Kärcher and Lohmann (2002) for the duration of the homogeneous nucleation event is

$$\tau_{freez}^{-1} = c\left(\frac{\partial \ln(J)}{\partial T}\right)_{S_i = S_{i,cr}} \frac{dT}{dt}. \tag{9}$$

In eq. (9), J is the nucleation rate and c represents a fit parameter. In KHL06 it is allowed for c to range between 0.8 and 1.5 depending on the ambient temperate, while Ren and MacKenzie (2005) propose $c = 1$. The derivative of the nucleation rate with respect to temperature is also needed for eq. (9). A simplified expression is derived in Ren and MacKenzie (2005), under the assumption that the nucleation rate is $J = 10^{10}$ cm^{-3} s^{-1} for the initial formation of ice particles per unit volume (see Appendix A.2.I). Following Ren and MacKenzie (2005) by inserting c, the adiabatic cooling rate and the parameterisation for the change of nucleation rate with temperature yields

$$\tau_{freez}^{-1} = [T(0.004T - 2) + 304.4]\frac{gw}{c_p}. \tag{10}$$

Combining eq. (8) and eq. (10) determines the onset (at t_{cr}) and end (at $t_{cr} + \tau_{freez}$) of the nucleation event. However, using eq. (9), the freezing event is found to be too short. This is shown by comparing τ_{freez} from eq. (10) to the duration of the freezing event simulated by the Koop parameterisation. The latter scheme is hereby considered to be the 'truth' as it uses a diagnostic nucleation rate based on a classical nucleation scheme and the ice crystal number density is explicitly calculated (see Appendix A.2.I). The time intervals of the freezing event from the Koop and the KHL06 scheme for $T = 220$ K and $w = 1$–1000 cm s^{-1} are depicted in Fig. 3. The time scale τ_{freez} from KHL06 is lower by a factor of 10 than τ_{freez} from the reference simulation (Koop et al., 2000), green and red line in Fig. 3, respectively. Multiplying τ_{freez} by a factor of 10 results in the modified KHL06 depicted by the blue line in Fig. 3. The introduction of this factor for the duration of the freezing event can be justified by the extended time it takes for an air parcel to reach equilibrium as opposed to a single ice crystal. Consequently, the nucleation event starts at t_{cr}

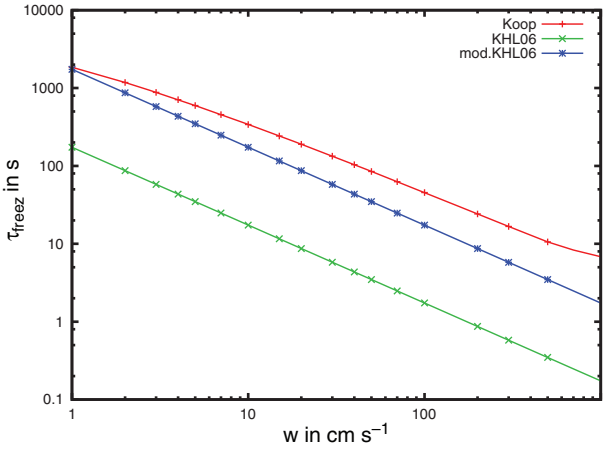

Fig. 3. The duration of the nucleation event τ_{freez} for an air parcel with $T = 220$ K and different vertical velocities depicted for the Koop, KHL06 and modified KHL06 scheme with the red, green and blue lines, respectively.

and ends at $t_{cr} + 10\tau_{freez}$. The nucleation event is thus completely captured within the next model time step if $\Delta t > (t_{cr} + 10\tau_{freez})$. It is crucial to include the longer freezing time scale, as t_{cr} becomes negative as soon as the nucleation event commences. In order to ensure that the ice supersaturation still lies above the critical ice supersaturation ratio in the next model time step, it is estimated by extrapolation (cf. KHL06)

$$S_i(t + \Delta t) = S_i + a_1 S_i (w - w_p)\Delta t \tag{11}$$

which also accounts for pre-existing ice crystals represented by the term w_p. Thus $t_{cr} + 10\tau_{freez}$ determines when and for how long a nucleation event occurs. The nucleation event takes place at the current time step only if the ice supersaturation is still above its critical value after the next model time step, that is, $S_i\,(t + \Delta t) > S_{i,cr}$.

In summary, the homogeneous nucleation event is triggered if all of the three following conditions are fulfilled simultaneously:

$$1)\ w > w_p \tag{12}$$

$$2)\ t_{cr} + 10\tau_{freez} < \Delta t \tag{13}$$

$$3)\ S_i(t + \Delta t) > S_{i,cr} \tag{14}$$

While (1) is already a predefined condition from KHL06, points (2) and (3) are newly implemented. These conditions lead to a physically based approach to capture the characteristic ice supersaturation overshoot occurrence in the parcel model, which is important for NWP models with a model time step of $\Delta t \approx \tau_{freez}$. Using only the original criteria from KHL06, namely, that the ice supersaturation exceeds $S_{i,cr}$ together with eq. (12), would cause the nucleation event to be triggered too soon. Higher ice

supersaturation values are possible through the extension of the criteria from eqs. (13) and (14), which is in accordance with the results from the Koop parameterisation and illustrated in Fig. 2. Through the new requirements eqs. (13) and (14) homogeneous freezing events are less frequent and the ice supersaturation attains higher values.

The comparison of the KHL06 scheme including the modification for the triggering of the homogeneous nucleation event to Koop et al. (2000) is shown in Fig. 2. A parcel model time step of $\Delta t = 1$ s and an adaptive time step around the nucleation event was used for the Koop et al. (2000) parameterisation. The parcel model was run with the time step $\Delta t = 1$ s for the KHL06 and the modified KHL06. It can be seen that the ice saturation curve shows the same behaviour for the explicitly resolved Koop et al. (2000) scheme as for the modified KHL06 scheme. Only implementing the KHL06 scheme would have caused a triggering of the nucleation event as soon as $S_{i,cr}$ is reached. In Haag et al. (2003) this higher peak in S_i above $S_{i,cr}$ is explained as a non-equilibrium effect which increases with decreasing temperature. This is due to slower ice particle growth and continuous cooling during the constant lifting of the parcel. Higher cooling rates result in a stronger non-equilibrium effect. Yet a stronger vertical updraft would result in a smaller freezing time interval when eq. (10) is used. The asymptotic value for $t \to \infty$ of the ice saturation ratio in Fig. 2 does not reach $S_i = 1$ due to the ongoing cooling of the air parcel resulting from the constant updraft. Through the new conditions listed as eqs. (13) and (14) the scheme becomes robust for larger time steps and the overshoot is captured. These conditions only hold under the assumption that the vertical velocity is sufficiently constant. Events might be missed for cases with high frequency fluctuations in the upper troposphere nucleation.

Due to the physically based behaviour, the KHL06 parameterisation became the scheme of choice and with the modifications it is robust enough for operational applications at a wide range of time steps. After the freezing event, the depositional time scale depicted in Fig. 2 becomes increasingly important.

2.4. Depositional growth

After nucleation sets in, the further development of the ice crystals is dominated by diffusional growth. The latter is coupled with the release of latent heat, causing an increase in buoyancy, which potentially increases vertical motion. This in turn directly affects the supersaturation, as it increases the water vapour supply for diffusional growth. This feedback motivates the necessity of an accurate physical description. The equations currently accounting for deposition in the DWD models will be explained and compared to different kinetic and thermodynamic approaches for spherical and hexagonal ice crystals. The resulting depositional time scales, along with a physical treatment for the ice crystal modes, will be discussed thereafter.

2.4.1. Kinetic and thermodynamic formulation. The time derivative of the cloud ice mixing ratio q_i with respect to depositional growth and for the ice mass m_i for an individual ice crystal is

$$\left.\frac{dq_i}{dt}\right|_{dep} = \frac{1}{\rho_a}\int_0^\infty \frac{dm_i(r_i)}{dt} f(x,y,z,r_i,t)\,dr_i \tag{15}$$

$$\text{with } \frac{dm_i}{dt} = 4\pi\rho_i r_i^2 \dot{r}_i \tag{16}$$

where $f(x, y, z, r_i, t)$ denotes the size distribution and $\int f(x, y, z, r_i, t)\, dr_i$ the ice crystal number density. In the ice microphysics scheme, the size distribution is assumed to be monodisperse, which simplifies the expression in eq. (15) to

$$\left.\frac{dq_i}{dt}\right|_{dep} = \frac{n_i \dot{m}_i}{\rho_a} = -\frac{4\pi}{\rho_a} = \rho_i n_i r_i^2 \dot{r}_i. \tag{17}$$

There are two different ways of formulating the depositional growth equation, namely the kinetic and thermodynamic formulation. The kinetic formulation is based on gas kinetics, where the statistical properties of molecules are considered. The thermodynamic formulation is based on macrophysical quantities and equilibrium states. These are equivalent formulations. However, for smaller ice crystals the kinetic formulation is favoured, while for larger ice crystals the thermodynamic formulation is commonly used. As discussed in Appendix B, the kinetic formulation for the change in cloud ice mixing ratio for the homogeneously nucleated ice crystals due to depositional growth is used.

$$\left.\frac{dq_i}{dt}\right|_{dep,hom} = \frac{\pi n_i r_i^2 m_w \alpha_d \nu_{th} e_{si}}{q_{v,si}\rho_a k_b T\left(1 + \frac{\alpha_d \nu_{th} r_i}{4D_v}\right)}\left(q_v - q_{v,si}\right) \tag{18}$$

For the larger, heterogeneously nucleated ice crystals the thermodynamically formulated depositional rate used in the regional COSMO model and global GME includes the form factor for hexagonal plates $a_{i,m} = 130$ kg m^{-3}. The diameter D_i is defined through the ice crystal mass $m_i = a_{i,m} D_i^3$ and is restricted to 200 μm in the models. Additionally, the Howell factor (Howell, 1949) H_i incorporates the effects due to the difference in ambient air and drop temperature and thus thermal diffusivity

$$\left.\frac{dq_i}{dt}\right|_{dep,het} = \frac{4\pi D_v D_i n_i}{1 + H_i}\left(q_v - q_{v,si}\right) \tag{19}$$

where

$$H_i = \frac{D_v L_s^2}{K_T R_v T^2} \rho_a q_{v,si}. \quad (20)$$

An extensive derivation and discussion can be found in Appendix B. In the following, the relationship between the kinetic and thermodynamic formulation is shown.

The question is to what extent the kinetic and thermodynamic formulation and ice crystal habit, that is, spherical or hexagonal plate, influence the ice crystal growth. In Fig. 4 the time evolution of ice crystal radii for the different depositional growth approaches is depicted in dependence of ambient atmospherical conditions favouring homogeneous (Fig. 4a) or heterogeneous (Fig. 4b) nucleation. The choice of the deposition coefficient α_d for the kinetic formulation from Kärcher and Lohmann (2002) is tested for $\alpha_d = 0.5$ and $\alpha_d = 0.05$. The deposition coefficient is one of the most uncertain parameters of the process and is especially important in the kinetic regime (Gierens et al., 2003). Typical values for α_d range from 0.005 to 1, where values lower than 0.1 lead to an insufficient depositional growth resulting in high cloud ice number concentrations and high ice supersaturations (Harrington et al., 2009). The spherical and hexagonal plate based on Khvorostyanov and Sassen (1998b) eq. (65) and the Howell formulation eq. (19) are considered for the thermodynamic approaches, respectively. For this plot the parcel model time step is set to $\Delta t = 1$ s and the air parcel is at rest, that is, with no updraft, where only the initial setting distinguishes the nucleation scenarios.

First, the evolution of an ice crystal with an initial radius of $r_{i,0} = 1\,\mu m$ resembling a homogeneous nucleated ice crystal size as shown in Fig. 4a is discussed. As diffusional growth occurs after the nucleation event is triggered, the critical ice supersaturation ratio eq. (7) is used for calculating the initial value for ice supersaturation for homogeneous freezing, which is $S_{i,cr} = 1.58$ for $T = 200$ K. The constant ice crystal number density $n_i = 10\ cm^{-3}$ is prone to occur in gravity wave scale updrafts of $w \approx 10\ cm\ s^{-1}$. It can be seen in Fig. 4a that depositional growth by use of the thermodynamic approach, that is, eqs. (65) and (19), depletes the ice supersaturation quickly, causing the asymptotic ice crystal radius $r_i = 3\,\mu m$ to be obtained at $S_i = 1$ within 250 s. In agreement with Harrington et al. (2009, a vast difference is noticeable when changing the deposition coefficient in eq. (62) from $\alpha_d = 0.5$ (Spichtinger and Gierens, 2009a) to $\alpha_d = 0.05$ (Stevens, 2011). Fukuta and Walter (1970) also comment that the kinetic growth approach resembles the Maxwellian equation when setting the deposition coefficient to one. This is because of the

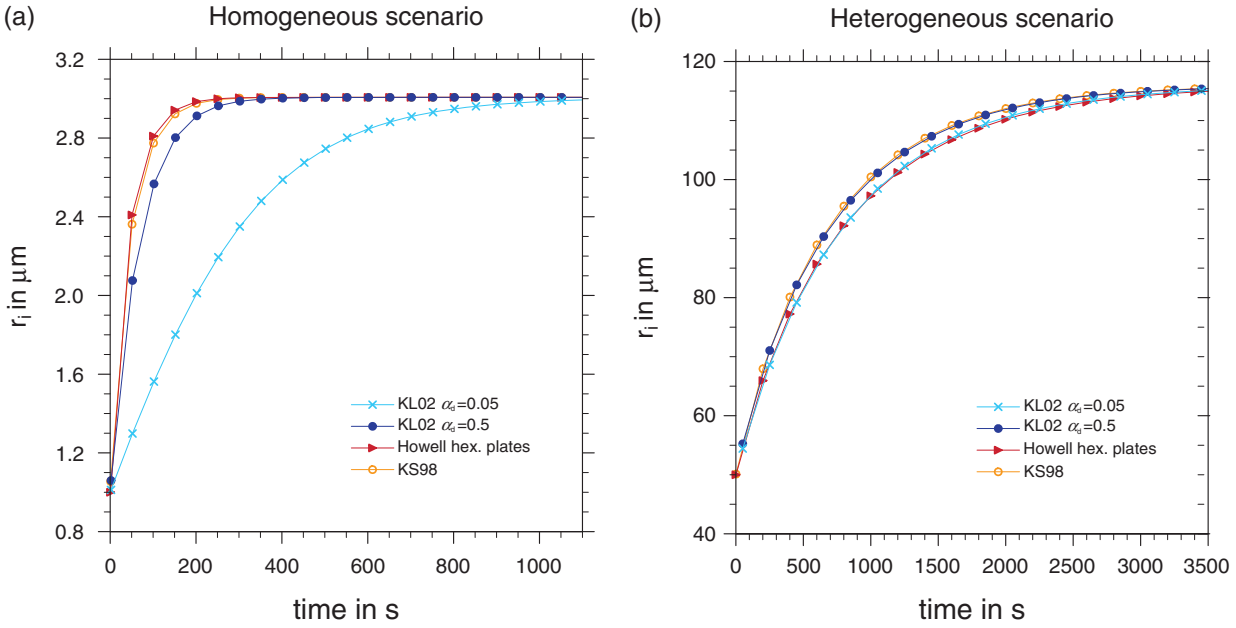

Fig. 4. The change in ice crystal radii over time for the (a) homogeneous and (b) heterogeneous scenario for the kinetic and thermodynamic depositional growth rates is depicted. For the homogeneous scenario, the initial ice crystal radius is $r_{i,0} = 1\,\mu m$, the ice crystal number density is set to $n_i = 10\ cm^{-3}$, and the temperature is $T = 200$ K. In the heterogeneous nucleation scenario, the initial ice crystal radius is $r_{i,0} = 50\,\mu m$, the constant ice crystal number density is $n_i = 10\ dm^{-3}$, and the temperature is set to $T = 240$ K. The pressure is $p = 240$ hPa for both scenarios. The dark and light blue lines show the influence of the deposition coefficient on the kinetic depositional growth rate. The ice crystal radii resulting from thermodynamic depositional growth rate considering spherical ice particles and hexagonal plates are shown in orange and red, respectively.

lower efficiency of diffusional growth with a lower deposition coefficient, causing ice supersaturation to reach higher values due to the slow depletion.

Using the critical nucleation threshold is not as simple for the heterogeneous freezing scenario, and it varies for different IN species. Thus for heterogeneous freezing conditions, the simplified freezing threshold

$$S_{\mathrm{w,cr}} = \left(\frac{T}{T_0}\right)^{\frac{M_{\mathrm{w}} L_{\mathrm{m}}^{ef}}{RT}} \tag{21}$$

is applied based on Khvorostyanov and Curry (2004), where L_{m}^{ef} is the effective latent heat of melting for which the approximation given in Khvorostyanov and Curry (2009) is used.

$$L_{\mathrm{m}}^{ef} = c_{\mathrm{L0}} + c_{\mathrm{L1}} T_{\mathrm{c}} + c_{\mathrm{L2}} T_{\mathrm{c}}^2 + c_{\mathrm{L4}} T_{\mathrm{c}}^4 \tag{22}$$

with $\mathrm{T_c}$ in °C and the dimensionless coefficients $c_{\mathrm{L0}} = 79.7$, $c_{\mathrm{L1}} = 0.333$, $c_{\mathrm{L2}} = -2.5 \times 10^{-3}$ and $c_{\mathrm{L4}} = 0.8 \times 10^{-7.}$ The critical ice saturation ratio for heterogeneous nucleation then results from $S_{\mathrm{i,cr}} = S_{\mathrm{w,cr}} e_{\mathrm{sw}}/e_{\mathrm{si}}$ and yields $S_{\mathrm{i,cr}} = 1.28$ for $T = 240$ K. The initial ice crystal number density is $n_{\mathrm{i}} = 10\ \mathrm{dm}^{-3}$, with the radius growing from $r_{\mathrm{i,0}} = 50$ μm to $r_{\mathrm{i}} = 115$ μm in 3500 s. As can be seen in Fig. 4b, there are no great differences between the kinetic, thermodynamic, spherical or hexagonal formulations.

Essentially, the kinetic formulation for diffusional growth shows a higher sensitivity towards the efficiency of the ice supersaturation depletion. While the larger heterogeneous particles accumulate more mass, the radius of the smaller homogeneous ice grows faster in comparison. Thus for homogeneously frozen ice crystals with small ice particle sizes comparable to the mean free path of air molecules, it is advisable to use the kinetic eq. (62). The thermodynamic approach coupled with the Howell factor as described by eq. (19) is applied to heterogeneous hexagonal ice crystal plates. These differences for the depositional growth motivate a coupled approach to model the competition between heterogeneously and homogeneously formed ice crystals for the available water vapour in an ice supersaturated environment. The coupled approach is pursued by use of the depositional growth time scales and investigated next.

2.4.II. Depositional growth time scale. A physical description for depositional growth is desirable, as it plays an important role in the depletion of ice supersaturation. The competition for water vapour between ice crystals developed by either homogeneous or heterogeneous freezing determines the ice particle number (DeMott et al., 1997). The competition highly depends on the time scale of diffusional growth for either cloud ice mode. The deposition time scale τ_{dep} was depicted in Fig. 2 and will be analysed subsequently.

The ice microphysics scheme in the NWP models of the DWD includes a limiter for the deposition rate. The maximum deposition rate is $(q_{\mathrm{v}} - q_{\mathrm{v,si}})/\Delta t$ in order to prevent more water vapour to be depleted than available after the depositional growth rate has been calculated. The use of such limiters motivates a more physical formulation of the depositional growth rate. Thus, it is desirable to distinguish the ice modes and to treat the depositional growth rates separately. A relaxation approach of the supersaturation towards an equilibrium state was already discussed in Gierens (2003), Korolev and Mazin (2003), Kärcher and Burkhardt (2008), as well as Wang and Penner (2010). However, the phase relaxation approach proposed in Morrison et al. (2005a) for high-resolution cloud models additionally includes the interaction between the hydrometeor species. This approach is adapted to the two-moment two-mode ice nucleation parcel scheme, where the number density $n_{\mathrm{i,x}}$ and cloud ice $q_{\mathrm{i,x}}$ are treated separately for $\mathrm{x} \in \{\mathrm{hom, het}\}$, respectively. The time scale indicates the ability of the air parcel to absorb vapour and the phase transition of vapour to ice. In this section, only the depositional time scale for cloud ice is accounted for, whereas later simulations include the further interaction of the depositional growth of snow [see eq. (38)]. The resulting equation for the depositional growth rate for the two-ice modes with their freezing time scales $\tau_{\mathrm{dep,x}}$ yields

$$\left.\frac{\Delta q_{\mathrm{i}}}{\Delta t}\right|_{\mathrm{dep,x}} = \frac{\chi(q_{\mathrm{v}} - q_{\mathrm{v,sat}})}{\tau_{\mathrm{dep,x}}} \left[1 - \exp\left(\frac{\Delta t}{\chi}\right)\right] \tag{23}$$

where χ is the general conjoined relaxation time

$$\chi = \left[(\tau_{\mathrm{dep,hom}}^{-1} + \tau_{\mathrm{dep,het}}^{-1})\right]^{-1}. \tag{24}$$

An interaction of the ice phases is accounted for through the joint time scale χ. The depositional time scale is

$$\tau_{\mathrm{dep,x}}^{-1} = \left.\frac{dq_i}{dt}\right|_{\mathrm{dep,x}} (q_{\mathrm{v}} - q_{\mathrm{v,si}})^{-1}. \tag{25}$$

The coupling of the diffusional relaxation time scales of the water vapour dependent ice phases thus serves as a more physical description. Also, a differentiation between the kinetic treatment of homogeneous spherical ice [eq. (62)] and the thermodynamic regime for hexagonal heterogeneous crystals [eq. (19)] is applied.

Because the change in cloud ice mixing ration with respect to deposition depends on q_{i}, n_{i} and r_{i} as seen in eq. (17), the time scales for different mean ice crystal radii and

number densities are investigated. In Fig. 5 the depositional time scale

$$\tau_{\mathrm{dep,het}}^{-1} = \frac{4\pi D_{\mathrm{v}} D_{\mathrm{i}} n_{\mathrm{i}}}{1 + H_{\mathrm{i}}} \tag{26}$$

is depicted for $T = 240$ K using the thermodynamic Howell equation (Howell, 1949) with hexagonal ice crystal shapes from eq. (19). The analogous change in ice crystal radius is depicted in Fig. 4b. Values for the time scales vary between $\tau_{\mathrm{dep,x}} = 0.24$ s for $r_{\mathrm{i}} = 500\,\mu$m and $n_{\mathrm{i}} = 10^4$ dm^{-3} and longer relaxation times of $\tau_{\mathrm{dep,x}} = 322$ hours for $r_{\mathrm{i}} = 1\,\mu$m and $n_{\mathrm{i}} = 1$ dm^{-3}. This shows how larger ice crystal radii and higher number densities reduce the depositional growth timespan. Ice crystal phase relaxation time scales are also noted in Table A1 from Khvorostyanov and Sassen (1998a) based on the thermodynamic approach with spherical particles, that is, $\tau_{\mathrm{dep}} = (4\pi D_{\mathrm{v}} n_{\mathrm{i}} r_{\mathrm{i}})^{-1}$. A comparison shows that $\tau_{\mathrm{dep,x}}$ shown in Fig. 5 is about 70% smaller than the time scales from Khvorostyanov and Sassen (1998a). This discrepancy is based on differing approximations of the diffusion coefficient D_{v} of water vapour in dry air. The formulation used in the parcel model was proposed by Pruppacher and Klett (1997) and is temperature and pressure dependent. It results in much higher D_{v} values for low atmospheric pressures than only temperature-related descriptions assuming sea level pressure, as used in Khvorostyanov and Sassen (1998a).

Using the depositional relaxation time scales in the new cloud ice scheme leads to a more physical approach and more realistic ice supersaturation values. The connection of the relaxation time scale to the quasi-stationary ice supersaturation state is approximated by Khvorostyanov and Sassen (1998a) with

$$(S_{\mathrm{i}} - 1)|_{\mathrm{eq}} = 1.1 \times 10^{-3} w \tau_{\mathrm{dep}} \text{ in } \%. \tag{27}$$

The equilibrium value thus results from the vertical updraft w in m s^{-1} and crystal phase relaxation time scale in s. This shows that intermediate values $n_{\mathrm{i}} = 100$ dm^{-3} and $r_{\mathrm{i}} = 100\,\mu$m mostly found at the top of cirrostratus (DeMott et al., 1994) have $\tau_{\mathrm{dep,x}} = 121$ s and $(S_{\mathrm{i}} - 1)|_{\mathrm{eq}} = 1.33\%$ for $w = 10$ cm s^{-1}. This indicates that no subsequent ice formation through homogeneous nucleation would take place and heterogeneous nucleation is dominant in such a regime (Khvorostyanov and Sassen, 1998a).

Not only the relaxation time scale approach, but also the application of the two-ice modes alters the depositional growth. The new relaxation time scale approach is coupled to the improved cloud ice scheme. This presents a more physical handling of the water vapour available for this process. Also, the possibility of competition for available water vapour between the ice modes and potentially snow is given. In the operational scheme, this was thus far neglected. The diffusional growth for the ice phases was calculated with the Euler forward scheme for time integration independently of each other with a limiter, ensuring that not more water vapour is depleted than available.

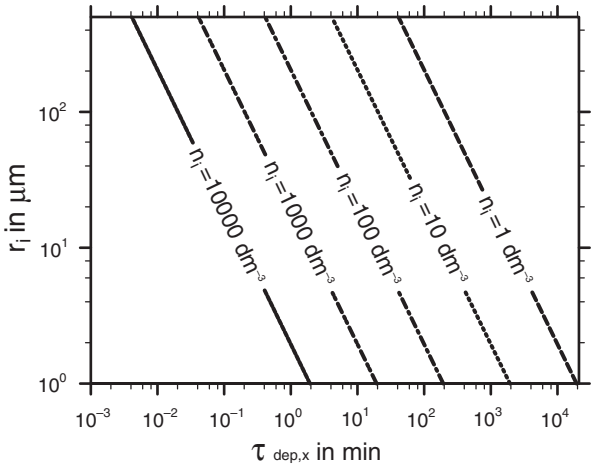

Fig. 5. The dependency of the depositional freezing time scale $\tau_{\mathrm{dep,het}}$ from eq. (19) on the mean ice crystal radius and number density for $T = 240$ K is shown.

2.5. *Interaction of nucleation processes*

In the proposed microphysics scheme, the previously introduced parameterisations for homogeneous and heterogeneous nucleation, as well as the changes for the depositional growth are included. This will allow a competition between the processes, which results in a more realistic approach. Depending on the ambient atmospheric conditions, that is, pressure, temperature, ice supersaturation, number of available IN and vertical velocity, either homogeneous, heterogeneous or both freezing mechanisms are triggered. An important aspect in correctly coupling the homogeneous and heterogeneous parameterisations are the different cirrus properties resulting from either regime. Heterogeneous nucleation potentially becomes dominant in contrail and cirrus regions with weak updrafts (Lin et al., 2002). Vertical velocities less than 20 cm s^{-1} are thought to be where heterogeneous nucleation has the maximum impact on cirrus cloud formation, whereas homogeneous nucleation gains importance at higher velocities (DeMott et al., 1997). The critical ice crystal number concentration needed in order to suppress subsequent homogeneous freezing is analytically derived by Gierens et al. (2003), their eq. (21), and also by Barahona and Nenes (2009), their eq. (20), for monodisperse IN based on cloud parcel model equations. The competition between the two nucleation

mechanisms in cirrus clouds was also investigated with 2-D simulations by, for example, Spichtinger and Gierens (2009b) and Joos et al. (2014).

A main objective in this work is to investigate the different behaviour of the operational parameterisations in the NWP models of the DWD and the new cloud ice nucleation scheme. However, as currently no parameterisation for homogeneous freezing of liquid aerosols is implemented, only the heterogeneous nucleation scheme from PDA08 is compared with the modified Fletcher equation, while for homogeneous freezing the KHL06 scheme with the modified trigger mechanism is used alone (see Table 2). In the following, the mutual interaction of the two nucleation schemes is investigated by using the parcel model with ambient temperature $T = 230$ K, pressure $p = 220$ hPa, constant vertical velocity $w = 40$ cm s^{-1} and model time step $\Delta t = 1$ s. Three scenarios are considered:

(1) no available ice nuclei (only homogeneous freezing)
(2) upper limit for the activated ice nuclei $\mathrm{IN}_{\max} = 100$ dm^{-3} (only heterogeneous freezing)
(3) upper limit of available ice nuclei $\mathrm{IN}_{\max} = 15$ dm^{-3} (heterogeneous and homogeneous freezing).

The model variables S_i, n_i, r_i and q_i for the three cases are compared in Fig. 6, where the green line represents the purely homogeneous freezing, the orange and red lines are the heterogeneous nucleation scenarios, and the light and dark blue lines show the interaction of both freezing mechanisms. In Fig. 6a the development of the ice supersaturation ratio over time is shown. The cloud ice mixing ratio in Fig. 6d results from adding the homogeneous and heterogeneously originated particles together. The mean ice crystal radius in Fig. 6c is defined by

$$r_\mathrm{i} = \frac{n_\mathrm{i,hom} r_\mathrm{i,hom} + n_\mathrm{i,het} r_\mathrm{i,het}}{n_\mathrm{i,hom} + n_\mathrm{i,het}} \tag{28}$$

to stress the differences in particle size for the two-ice modes and number densities in Fig. 6b. This definition also explains the gap with abrupt change in Fig. 6c and b.

First, the ice supersaturation ratios and ice crystal number densities for the solely heterogeneous and homogeneous nucleation cases are regarded. The latter case is represented by the green line in Fig. 6. The homogeneous nucleation event is triggered near the critical ice supersaturation ratio $S_\mathrm{i,cr} = 1.47$ at $S_\mathrm{i} = 1.5$ (Fig. 6a) and the resulting ice crystal number density is $n_\mathrm{i} = 594$ dm^{-3}. Clear differences are visible when comparing the two heterogeneous nucleation schemes with an available number density of ice nuclei $\mathrm{IN}_{\max} = 100$ dm^{-3}. The ice crystal number concentration resulting from the modified Fletcher equation causes all the available IN to be activated at once, reaching the limit $n_\mathrm{i,het} = 100$ dm^{-3} within the first time step (Fig. 6b), and quickly depletes the ice supersaturation to its asymptotic value (Fig. 6a). This quick activation of all IN does not occur when using the PDA08 scheme, as the IN are gradually activated over time until $n_\mathrm{i,het} = 29$ dm^{-3}. Thus, not all 100 dm^{-3} available IN are activated. The low ice crystal number density of 29 dm^{-3} is not able to efficiently reduce the ice supersaturation (Fig. 6a) if homogeneous nucleation is unphysically suppressed. However, this scenario clearly demonstrates the difference in IN activation between the two heterogeneous nucleation schemes. The operational NWP scheme thus easily overestimates the activated IN for the amount of background aerosol available.

With help of Fig. 6 the interaction of the homogeneous nucleation scheme in conjunction with the modified Fletcher equation and the PDA08 scheme is depicted with the light and dark blue lines, respectively. The available IN number density is $\mathrm{IN}_{\max} = 15$ dm^{-3}. The higher the ice crystal number density resulting from the heterogeneous nucleation, the later homogeneous nucleation is triggered. This clearly shows the competition between decreasing ice supersaturation due to existing ice crystals and its increase because of the air parcel's constant lifting, depicted in Fig. 6a. The ice crystal radius (Fig. 6c) plays a great role as well, as the larger heterogeneous ice particles grow slower than the smaller homogeneous ice crystals, but deplete the ice supersaturation quicker due to their larger surface area. This is clearly depicted in Fig. 6a as the heterogeneously nucleated particles from the modified Fletcher equation cause homogeneous freezing to be postponed. The cloud ice mixing ratios q_i are shown in Fig. 6d. While there are great differences in q_i for all cases under 2000 s, afterwards they asymptotically approach the dashed black line, which is the cloud ice mixing ratio for saturation $q_\mathrm{i,sat}$. This result already indicates that for regions with mature cirrus clouds or with persistent updraft, the cloud ice mixing ratio is going to be similar for all ice nucleation schemes. Yet in Fig. 6d for $t < 2000$ s the discrepancy between the schemes is the most pronounced, which leads to the conclusion that the new ice nucleation parameterisations have the greatest impact on cirrus clouds that have not yet reached thermal equilibrium. In particular, the cloud ice mixing ratios from the heterogeneous nucleation case depicted by the red and orange line in Fig. 6d differ to a large extent. Choosing the modified Fletcher's equation (red line), as the NWP models of the DWD currently do, the cloud ice mixing ratios are overestimated for $t < 1000$ s.

In summary, homogeneous freezing produces ice particles with smaller radii but larger number densities, while heterogeneous nucleation generates larger but fewer ice particles. Consequently, the choice of ice nucleation parameterisation needs to be carefully considered. This choice is especially crucial for the cloud properties of non-equilibrium cirrus.

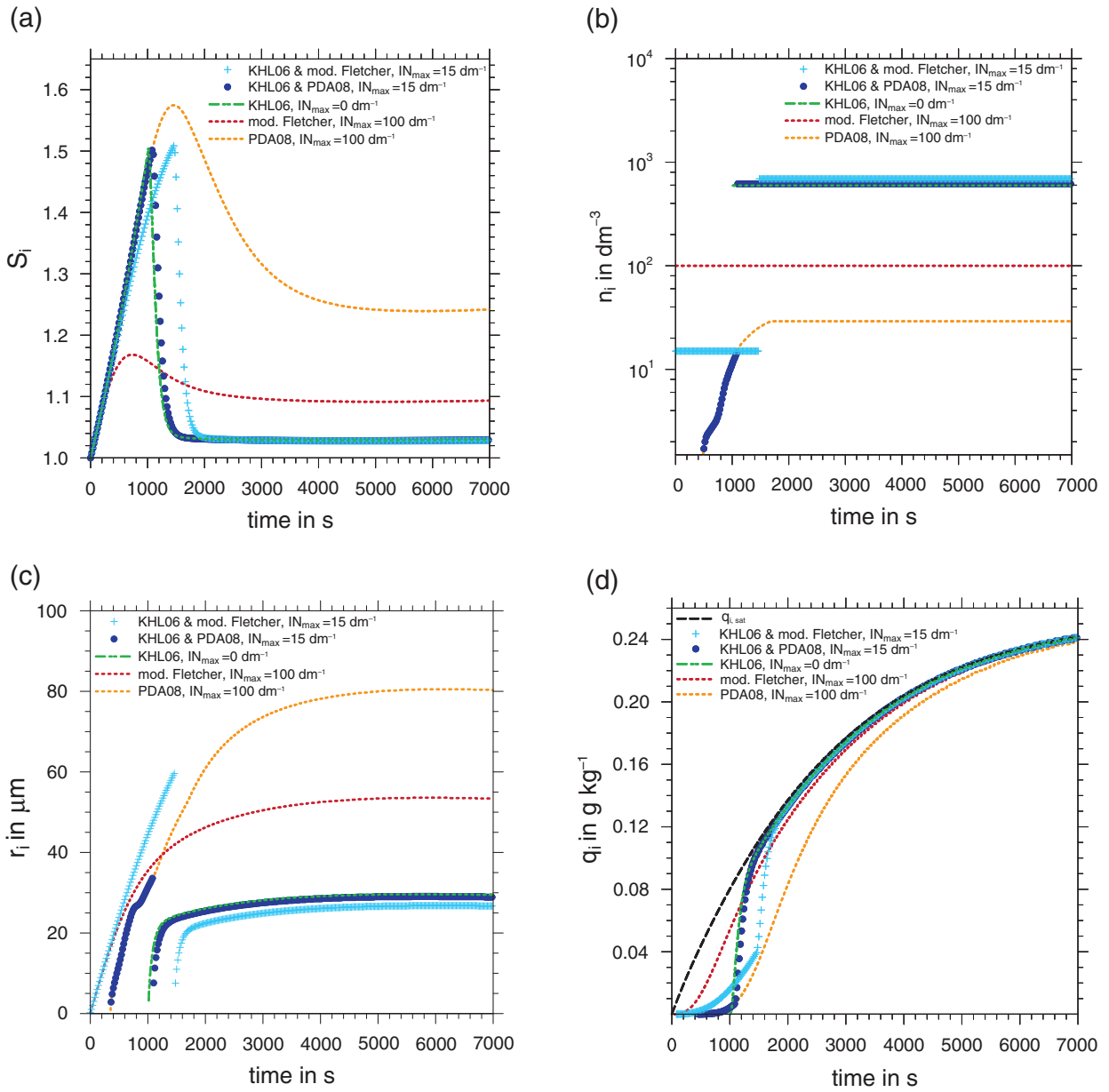

Fig. 6. Parcel model simulations with the initial values for the temperature $T = 230$ K, the pressure $p = 220$ hPa and the vertical velocity $w = 40$ cm s^{-1}, which reveal the characteristics of homogeneous and heterogeneous nucleation, as well as their interaction. The KHL06 homogeneous nucleation scheme is used, combined once with the heterogeneous schemes applying the modified Fletcher equation and once with PDA08. Different confining maximum values for $n_{i,het}$ and $n_{i,hom}$ lead to the competition between the two processes (light and dark blue symbols), purely homogeneous freezing (green line) and solely heterogeneous nucleation (orange and red lines for PDA08 and the modified Fletcher equation, respectively). In (a) the ice supersaturation ratio, (b) the ice crystal number density, (c) the ice crystal radius and (d) the cloud ice mixing ratio for the two modes are shown. In (d) the cloud ice mixing ratio for saturation is depicted by the dashed black line.

3. COSMO model framework

In order to fully understand the microphysical processes in cirrus clouds, it is important to perform high-resolution simulations in an NWP model environment. Thorough tests of the new cloud ice nucleation scheme in a parcel model were followed by idealised simulations with a horizontal resolution of 1 km. The advantage of such simulations lies in the well-defined environment where modifications can be performed in a straightforward manner. By varying the initial values, sensitivities can be better understood and parameter studies conducted.

The new nucleation parameterisations are implemented in the two-category ice cloud scheme that is currently operational in the COSMO. A brief overview and the basic model equations are given. Further modifications were included for a more physical description of the ice controlling factors. These include fluctuations of the vertical velocity, a budget variable for activated IN and sedimentation of ice crystals. Furthermore, the new treatment for the diffusional growth of cloud ice from Section 2.4.II is extended by snow.

The relevant processes in the COSMO concerning cloud ice will be discussed as described in the COSMO documentation (Doms et al., 2007). The bulk-water continuity model is based on the prognostic equations for the mass mixing ratios of the different hydrometeors: cloud water q_c, cloud ice q_i, rain q_r and snow q_s in kg kg^{-1}.

The generic budget equation for the mass mixing ratios in advection form is

$$\frac{\partial q_j}{\partial t} + \vec{v} \cdot \nabla q_j - \frac{1}{\rho_a} \frac{\partial}{\partial z}(\rho_a q_j v_j^T) = S_j - \frac{1}{\rho_a} \nabla \cdot F_j \qquad (29)$$

where $j \in \{c,\ i,\ r,\ s\}$ and S_j are the cloud microphysical sources and sinks per unit mass of moist air. F_j denotes the turbulent fluxes and v_j^T the mean terminal velocities of the particles of the precipitation and sedimentation fluxes. For the time being, cloud water q_c and cloud ice q_i are considered to be non-precipitating, thus having a negligible fall velocity in the operational model setup. The sedimentation flux $\frac{1}{\rho_a} \frac{\partial}{\partial z} (\rho_a q_{c,i} v_{c,i}^T)$ is therefore currently neglected.

The conservation equations for the two-category one-moment ice scheme for the mixing ratios of cloud water, cloud ice, rain and snow as stated in Doms et al. (2007) read:

$$\frac{\partial T}{\partial t} = A_T + \frac{L_v}{c_{pd}}(S_c + S_r) + \frac{L_s}{c_{pd}}(S_i + S_s) \qquad (30)$$

$$\frac{\partial q_k}{\partial t} = A_{q_k} + S_k \qquad (31)$$

$$\frac{\partial q_m}{\partial t} = A_{q_m} + \frac{1}{\rho_a} \frac{\partial}{\partial z}(\rho_a q_m v_m^T) = S_m. \qquad (32)$$

with $k \in \{i,\ c\}$ and $m \in \{s,\ r\}$. The advection terms A_T, A_{q_k}, and A_{q_m} also summarise other processes, for example, turbulent diffusion. The term L_v states the latent heat of evaporation and c_{pd} the specific heat capacity for dry air. As cloud ice is of primary interest in this work, the source and sinks for this category are described in detail below.

3.1. Two-moment two-mode variables

Additional prognostic model variables are implemented in order to better treat the homogeneous and heterogeneous ice nucleation processes. The mass fractions are treated separately for the heterogeneous and homogeneous evolved cloud ice modes. The changes of the cloud ice mixing ratios $q_{i,x}$ and ice crystal number densities $N_{i,x}$ with $x \in \{hom,\ het\}$ are calculated by use of the source and sink terms stated in Table 1.

$$\left.\frac{\partial q_i}{\partial t}\right|_x = S_{nuc} + S_{frz} + S_{dep} - S_{melt} - S_{cri} - S_{agg} - S_{au} \qquad (33)$$

$$\left.\frac{\partial N_i}{\partial t}\right|_x = S_{nuc} + \frac{S_{frz}}{\bar{x}_c} - \frac{S_{melt} + S_{cri} + S_{agg} + S_{au}}{\bar{x}_i} \qquad (34)$$

where $\bar{x}_c$ is the average mass of cloud droplets and $\bar{x}_i = q_{i,x}/N_{i,x}$ is the average mass of the cloud ice mode considered. All of the above noted terms are thus evaluated according to the two-ice modes, respectively. The source and sink terms that are not described in the course of this study are all consistent with the operational scheme documented in Doms et al. (2007). In the operational cloud ice scheme, the cloud ice sink S_{aud} is also included, which is the autoconversion of cloud ice to form snow due to depositional growth.

$$S_{aud} = \frac{S_{i,dep}}{1.5(m_{s,0}/m_i)^{2/3} - 1} \qquad (35)$$

where $m_{s,0} = 3 \times 10^{-9}$ kg is the initial mass for snow crystals equivalent to $D_{s,0} = 300\,\mu$m. This process can reduce the ice crystal depositional growth rate by as much as 65%. Changes in the depositional growth equation described in Section 3.4 and the use of a two-moment formulation suggest abandoning this autoconversion term. Thus, S_{aud} is not considered further on.

3.2. Fluctuations induced by turbulent kinetic energy

Homogeneous nucleation is strongly dependent on high cooling rates triggered by high vertical velocities. Thus, upper-tropospheric fluctuations in the wind field would be desirable. For this purpose the turbulent kinetic energy (*TKE*) is applied as a sub-grid scale velocity for ice nucleation, see, for example, Joos et al. (2008) and Gettelman et al. (2010). The TKE is treated as a prognostic variable in

Table 1. Cloud ice sources and sink terms used in the COSMO model

S_{nuc}	Nucleation of cloud ice (het. or hom.)
S_{frz}	Nucleation of cloud ice due to hom. freezing of cloud water
S_{dep}	Deposition growth and sublimation of cloud ice
S_{melt}	Melting of cloud ice to form cloud water
S_{au}	Autoconvers of cloud ice to form snow due to aggregation
S_{aud}	Autoconvers of cloud ice to form snow due to deposition
S_{agg}	Collection of cloud ice by snow (aggregation)
S_{cri}	Collection of ice by rain to form snow

the COSMO model, as opposed to its diagnostic treatment in the global model GME. This makes it possible to account for vertical diffusion and TKE production through sub-grid scale thermal circulation in the COSMO model (Baldauf et al., 2011). The TKE scheme therein is based on a hierarchy order 2.5 closure model (based on the classifications introduced by Mellor and Yamada, 1974).

Following Lohmann et al. (1999a), the vertical velocity used in the proposed cloud ice scheme is calculated from the square root of the *TKE* and a scalable factor. In the climate model ECHAM5 (European Center Hamburg, version 5), the relation $w_{\mathrm{TKE}} = 0.7\sqrt{TKE}$ for sub-grid scale fluctuations, which is based on an isotropic assumption, is applied (Joos et al., 2008). This assumption is implemented into the COSMO model with a reduced factor $w_{\mathrm{TKE}} = 0.5\sqrt{TKE}$. In Lohmann et al. (1999b), the pre-factor ranges between 0.5 and 1 with low sensitivities. In this work, we chose the lower value of 0.5 for the regional COSMO model, as opposed to the global model used by Lohmann et al. (1999a). The total vertical velocity for the ice nucleation scheme thus results in $w = w_{\mathrm{COSMO}} + w_{\mathrm{TKE}}$, where w_{COSMO} is the vertical velocity in the COSMO model.

3.3. IN budget variable for heterogeneous nucleation

In the heterogeneous nucleation scheme by PDA08, a constant number concentration for each of the three aerosol species is assumed. However, IN are unevenly distributed in the upper atmosphere. A more sophisticated way to represent IN in the cloud ice scheme would be to use a coupled prognostic aerosol model, such as the COSMO-ART (Aerosol and Reactive Trace gases) (Vogel et al., 2009). Such an interactive aerosol and extensive model would be numerically too expensive for operational use at this time. However, the fixed number of available IN is not realistic and would lead to an overestimation of the number of heterogeneously nucleated ice crystals. A prognostic budget variable for activated IN is introduced to prohibit such an overestimation of nucleated ice crystals due to the amount of predetermined IN. The budget variable $N_{\mathrm{i,nuc}}$ is introduced in order to limit newly nucleated heterogeneous ice and account for activated IN. A similar approach is used by Cohard and Pinty (2000) for cloud condensation nuclei and, for example, in Phillips et al. (2007) for IN.

The predefined aerosol number density from PDA08 serves as an initial value and remains constant over all time steps. The available IN are reduced by previously nucleated IN represented by the heterogeneous cloud ice number concentration $N_{\mathrm{i,het}}$. The prognostic formulation of the activated IN number concentration $\mathrm{N_{i,nuc}}$ per unit mass reads

$$\frac{\partial N_{\mathrm{i,nuc}}}{\partial \mathrm{t}} + v \cdot \nabla N_{\mathrm{i,nuc}} = \left.\frac{\partial N_{\mathrm{i,het}}}{\partial t}\right|_{\mathrm{nuc}} - \frac{N_{\mathrm{i,nuc}}}{\tau_{\mathrm{mix}}} \qquad (36)$$

where τ_{mix} is a mixing time scale. This time scale is an estimation for the mixing in the atmosphere, after which new IN would be available for heterogeneous nucleation. The mixing time scale τ_{mix} is derived from the turbulence time scale $\tau = TKE^{-1/2}l$, where l is the turbulence length scale (Mironov, 2009). This approach for estimating the mixing time scale mostly holds for the lower troposphere and warm, that is, ice free, clouds, and is discussed in Andrejczuk et al. (2009) and references therein. With upper air TKE values between 0.0005 and 0.005 $\mathrm{m^2\ s^{-2}}$ and a length scale for eddy sizes of 300 m the mixing time scale results in $\tau_{\mathrm{mix}} \approx 1$–4 hours. Throughout this study τ_{mix} is set to 4 hours. Increasing the mixing time scale reduces the available IN, while reducing it causes more IN to be available. In the following, the maximum value for activated IN is set to $\mathrm{IN_{max}} = 50\ \mathrm{dm^{-3}}$, that is, a maximum heterogeneous cloud ice concentration of $N_{\mathrm{i,het}} = 50\ \mathrm{dm^{-3}}$. Heterogeneous nucleation is only triggered if there are still unactivated IN available for further nucleation, that is, under the condition that $N_{\mathrm{i,nuc}} < N_{\mathrm{het,max}}$. The IN budget equation eq. (36) thus provides a prognostic approach to trace previously activated IN without being numerically too costly. This is a simplified approach to account for so-called nucleation scavenging (Morrison et al., 2005b). The IN tracking thus increases the spatial variability of IN. It reduces the amount of unactivated/background IN and removes the false advantage for heterogeneous nucleation.

3.4. Depositional growth including snow

The depositional growth of cloud ice was discussed in detail in Section 2.4. In the COSMO model, snow also depends on the water vapour resources for deposition and is included in the new depositional growth formulation. The operational depositional growth equation for snow is

$$\left.\frac{dq_{\mathrm{s}}}{dt}\right|_{\mathrm{dep}} = \frac{4D_{\mathrm{v}}n_{\mathrm{s,0}}}{1+H_{\mathrm{i}}}(1+c_{\mathrm{dep}})\ (q_{\mathrm{v}} - q_{\mathrm{v,si}}) \qquad (37)$$

where c_{dep} depends on $\rho_{\mathrm{a}}q_{\mathrm{s}}$, the gamma function and assumptions concerning the terminal velocity (Doms et al., 2007). In eq. (37), $n_{\mathrm{s,0}}$ is a temperature dependent coefficient based on second moment relations and mass-size relation from Field et al. (2005) and described in Seifert (2008). Following Morrison et al. (2005a) yields the formulation of the relaxation time scales analogue to eqs. (23) and (24) for the change of the cloud ice modes and snow mixing ratios with respect to depositional growth

$$\left.\frac{dq_{\mathrm{i,s}}}{dt}\right|_{\mathrm{dep,x}} = -\frac{\chi(q_{\mathrm{v}} - q_{\mathrm{si}})}{\tau_{\mathrm{dep,x}}\,\Delta t}\left[1 - \exp\left(\frac{-\Delta t}{\chi}\right)\right] \qquad (38)$$

with $x \in \{hom,\ het,\ snow\}$ and the general deposition relaxation time

$$\chi = \left[\tau_{\mathrm{dep,hom}}^{-1} + \tau_{\mathrm{dep,het}}^{-1} + \tau_{\mathrm{dep,snow}}^{-1}\right]^{-1}. \tag{39}$$

This is the formulation for the deposition rate for the cloud ice modes and snow.

3.5. Cloud ice sedimentation

In the operational DWD NWP models, ice crystals are considered non-precipitating; that is, the process of sedimentation is neglected. Yet its importance is emphasised in the studies of, for example, Spichtinger and Gierens (2009a) and Spichtinger and Cziczo (2010). In the latter, it is stated that the high ice supersaturation found in cirrus clouds are a potential feedback of sedimentation, as the ice crystals fall out prior to ice supersaturation depletion. The impact of the ice crystal terminal velocities on the build-up and decay of cirrus clouds is also stressed by Heymsfield and Iaquinta (2000), while Jensen et al. (2011) highlight its limiting effect due to radiative–dynamic interactions. The implementation of cloud ice sedimentation in the ECMWF global model and its effect on radiation is discussed by Jakob (2002). Therefore, it is important to include this process in the new cloud ice scheme.

Cloud ice fall velocities are often formulated as empirical functions of the specific ice content (Jakob, 2002) or of temperature and pressure (Heymsfield and Iaquinta, 2000). Alternatively, the mass-dimension m–D and area-dimension A–D relations can be used,

$$m = \alpha D^{\beta} \quad \text{and} \quad \mathrm{A} = \gamma D^{\sigma} \tag{40}$$

where D is the maximum dimension, α and β the mass-size and γ and σ the area-size relation exponents depending on the geometry.

To account for cloud ice sedimentation in the present study, the sedimentation velocity v_{i}^{T} is introduced into the prognostic equations. The eq. (31) is extended by the sedimentation flux using the terminal velocity v_{i}^{T} for the homogeneous and heterogeneous cloud ice mixing ratios $q_{\mathrm{i,x}}$. The same is done for their ice crystal numbers $N_{\mathrm{i,x}}$

$$\frac{\partial q_{\mathrm{i,x}}}{\partial t} = \mathrm{A}_{\mathrm{q_{i,x}}} + \frac{1}{\rho}\frac{\partial}{\partial z}\left(\rho q_{\mathrm{i,x}} v_{\mathrm{i}}^{T}\big|_{\mathrm{x}}\right) + S_{\mathrm{i}}\big|_{\mathrm{x}}, \tag{41}$$

$$\frac{\partial N_{\mathrm{i,x}}}{\partial t} = \mathrm{A}_{\mathrm{N_{i,x}}} + \frac{1}{\rho}\frac{\partial}{\partial z}\left(\rho N_{\mathrm{i,x}} v_{\mathrm{i}}^{T}\big|_{\mathrm{x}}\right) + S_{\mathrm{i}}\big|_{\mathrm{x}}, \tag{42}$$

where $A_{\mathrm{q_{i,x}}}$ and $A_{\mathrm{N_{i,x}}}$ represent the advection terms and $S_{\mathrm{i}}|_{\mathrm{x}}$ the source terms for both ice modes. In eqs. (41) and (42), the terminal velocity v_{i}^{T} is the same for the number of ice crystals and the cloud ice mixing ratio as the assumption of monodisperse particles is made. This results in the full model equations for the new cloud ice scheme for the COSMO model. The terminal velocity formulation proposed by Khvorostyanov and Curry (2005) is implemented. An overview of this scheme is given in Appendix A.3. By using this scheme, terminal velocities for different geometries, namely hexagonal plates, bullet rosettes and hexagonal columns and their equivalent diameters are depicted in Fig. 7 using the reference air density $\rho_{\mathrm{a}} = 1.225$ kg m^{-3}. Hexagonal plates are assumed for heterogeneously nucleated ice, while spherical particles are assumed for homogeneously nucleated ice particles. These geometries were already chosen for the depositional growth and are thus consistent.

4. Idealised COSMO model simulations of orographic cirrus

In the previous Sections 2 and 3, the framework for the new cloud ice microphysics scheme was explained and summarised in Table 2. Also, further prognostic model variables were implemented for the two-moment two-modes, along with an additional budget variable for activated IN. The whole cloud ice scheme is now tested within the COSMO model environment and sensitivities towards the modifications are investigated. Previous work, for example, by Joos et al. (2014), has thoroughly studied the interaction of homogeneous and heterogeneous nucleation in an idealised single mountain setup. For a more complex gravity wave pattern our artificial model orography h_{surf} consists of five bell-shaped hills with half-width $a = 20$ km

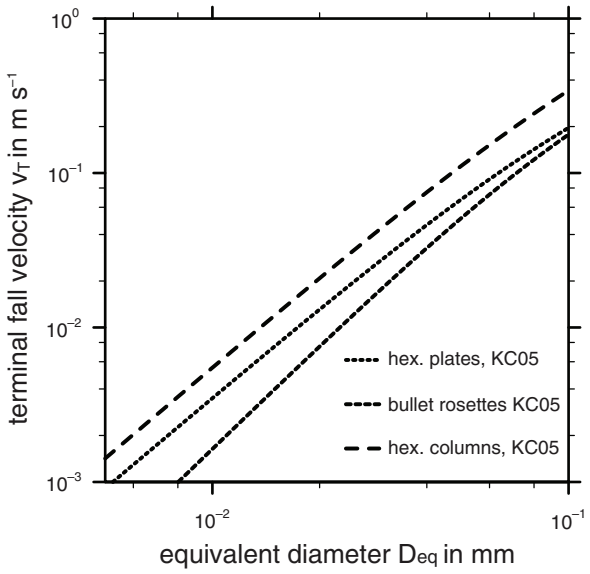

Fig. 7. The plot depicts the terminal velocities for different ice crystal shapes based on Khvorostyanov and Curry (2005) with the reference air density $\rho_{\mathrm{a}} = 1.225$ kg m^{-3}.

Table 2. Overview of the new and operational cloud ice nucleation scheme

	Operational parameterisations	New parameterisations
Prognostic variables	q_i	$q_{i,hom}$, $q_{i,het}$, $N_{i,hom}$, $N_{i,het}$, $N_{i,nuc}$
Homogeneous nucleation	–	Kärcher et al. (2006)
Heterogeneous nucleation	Modified Fletcher (1962)	Phillips et al. (2008)
Vertical velocity	$w = w_{COSMO}$	$w = w_{COSMO} + w_{TKE}$
Depositional growth	Howell (1949) with Euler forward and limiter	Morrison et al. (2005a)
Cloud ice sedimentation	–	Khvorostyanov and Curry (2005)

and height h_{max}. The surface topography in the x-direction is given by

$$h_{surf}(x) = \sum_{n=1}^{5} \frac{h_{max}}{\left(\frac{((x/2-1)-(n-3)3a)^2}{a^2}+1\right)^2}. \quad (43)$$

Gravity waves develop due to an initial horizontal wind speed of $u_0 = 12$ m s^{-1}. The idealised simulations have a horizontal resolution of $\Delta x = 1$ km, 99 vertical layers and a time step of $\Delta t = 8$ s are run for 12 hours. Additionally, a 2 km deep layer between 9 and 11 km is initialised with a relative humidity with respect to ice of $RH_i = 130\%$. This setup is illustrated in Fig. 8 after a model run time of 8 hours. It shows RH_i (Fig. 8a) and the vertical velocity w (Fig. 8b) for a mountain height of 1 km along with the isolines.

The main factors controlling cirrus cloud properties are the variability in vertical velocity and the existence of background aerosols (e.g. Haag and Kärcher, 2004). The topography height influences the intensity of gravity waves, where higher height leads to stronger orographic forcing. In order to investigate the effect of IN on the development of cirrus clouds, a factor χ_{IN} is introduced as a scaling parameter for the amount of available IN, that is, for $n_{DM} = 162$ dm^{-3}, $n_{BC} = 15$ cm^{-3} and $n_O = 1.77$ cm^{-3}. Setting this factor to $\chi_{IN} = 1$ results in the IN quantity proposed in Phillips et al. (2008). While stronger updrafts trigger homogeneous freezing of liquid aerosols, the number of IN in the atmosphere governs the heterogeneous nucleation. Haag and Kärcher (2004) state that 0.01 cm^{-3} IN are a threshold number concentration, above which the heterogeneous nucleation process becomes dominant and the role of homogeneous nucleation is diminished. Even though this value is strongly dependent on the ambient temperature, the cooling rate and the IN freezing need to be further investigated as the controlling factors. Thus, the sensitivity of the ice nucleation processes towards the orographic forcing and available IN is investigated by varying the maximum mountain height h_{max} and the scaling factor for IN χ_{IN}. So with h_{max} the ice supersaturation is scaled and with χ_{IN} the amount of available IN.

In the following, the competition between the ice nucleation mechanisms for the availability of IN as opposed to the effects of the vertical velocity magnitude induced by gravity waves is compared. As an example, an intermediate setup with $h_{max} = 1$ km and $\chi_{IN} = 0.3$ is shown in Fig. 8, in which both nucleation mechanisms are triggered. It shows the number densities for homogeneous freezing $n_{i,hom}$ (Fig. 8c) and heterogeneous nucleation $n_{i,het}$ (Fig. 8d). When looking at a regime where the two modes are active, the different characteristics of the freezing mechanisms become clearly visible. The mean cloud ice number density $n_{i,het} = 0.19$ dm^{-3} and maximum $n_{i,het} = 16.58$ dm^{-3} is much lower than for homogeneous freezing, where the mean value is $n_{i,hom} = 2.05$ dm^{-3} and maximum $n_{i,hom} = 1852.91$ dm^{-3}. The thicker, homogeneously formed cirrus are situated in the regions of strong updraft and consequently high ice supersaturation values. Also, the cloud ice mean diameter is much smaller in the regions of strong updraft, that is, regions in which homogeneous nucleation was triggered, while maximum values of $D_i \approx 150$ µm are obtained, where only heterogeneous nucleation was active (not shown). This reduction of the number of ice crystals and subsequent increased effective cloud ice radii is the key effect of IN on cirrus clouds (Haag and Kärcher, 2004). Figure 8c and d also show that a denser cirrus cloud forms after the first mountain, while the subsequent orographic cirrus are smaller. Due to the horizontal velocity in the upper troposphere, the cirrus clouds drift to the right of the model domain. The number densities for the homogeneously nucleated cloud ice is much lower in this region and could easily be mistaken for having a heterogeneous freezing origin. This clarifies the importance to separate the two cloud ice nucleation modes in order to identify the sensitivities for each mode.

IN in the atmosphere are a necessity for the triggering of heterogeneous freezing. Thus, the limitation of available IN by a simplified IN budget has a large impact on cirrus cloud formation. The heterogeneously nucleated ice particles are larger, making them susceptible to sedimentation, which alters the cirrus cloud properties. The impact of the tracking of activated IN for a mixing time scale of $\tau_{mix} = 4$ hours and cloud ice sedimentation are shown exemplarily in Fig. 9. The simulation result after 12 hours is plotted, at which a quasi-stationary state is reached. The mountain height of $h_{max} = 0.8$ km and aerosol scaling factor $\chi_{IN} = 3$

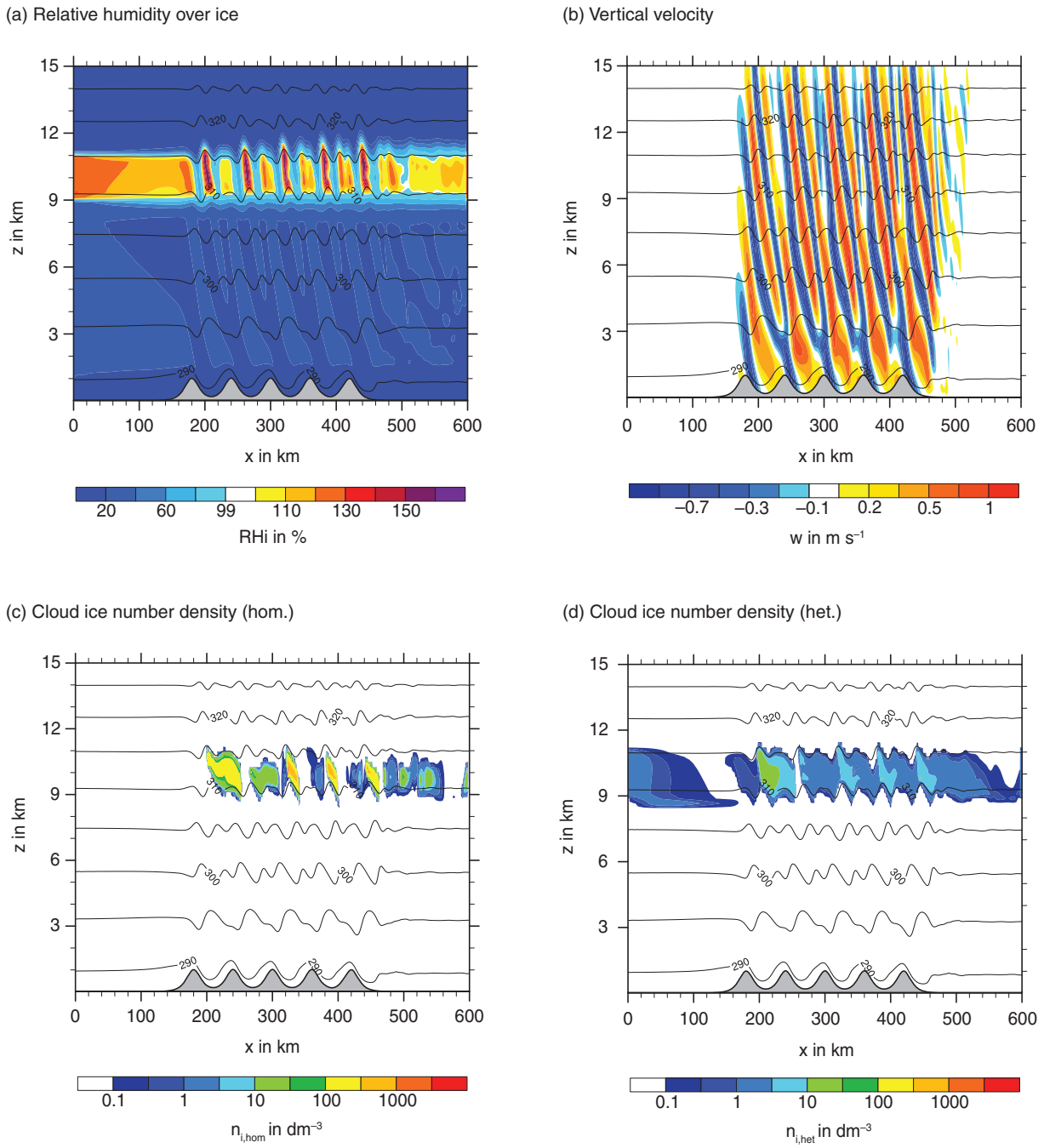

Fig. 8. A 2 km broad layer between 9 and 11 km is initialised with $RH_i = 130\%$ where the relative humidity with respect to ice is shown in (a) after the simulation time of 8 hours. The initial conditions for this idealised simulation are $RH_i = 130\%$, $h_{max} = 1$ km, $u_0 = 12$ m s^{-1} and $\chi_{IN} = 3$, causing both nucleation regimes to be triggered. High vertical velocities in gravity waves are achieved through strong orographic forcing, with the vertical velocity depicted in (b). The cloud ice number density for homogeneous and heterogeneous nucleation are shown in (c) and (d), respectively.

result in a heterogeneous freezing dominated scenario. Figure 9a includes the effect of IN tracking and cloud ice sedimentation in the cloud ice scheme. The corresponding number density of the tracking variable $n_{i,nuc}$ is plotted in Fig. 9b. Not tracking the activated IN means assuming a constant amount of available atmospheric IN in every time step. In Fig. 9c the budget variable is not included and thus the amount of heterogeneously nucleated particles is higher

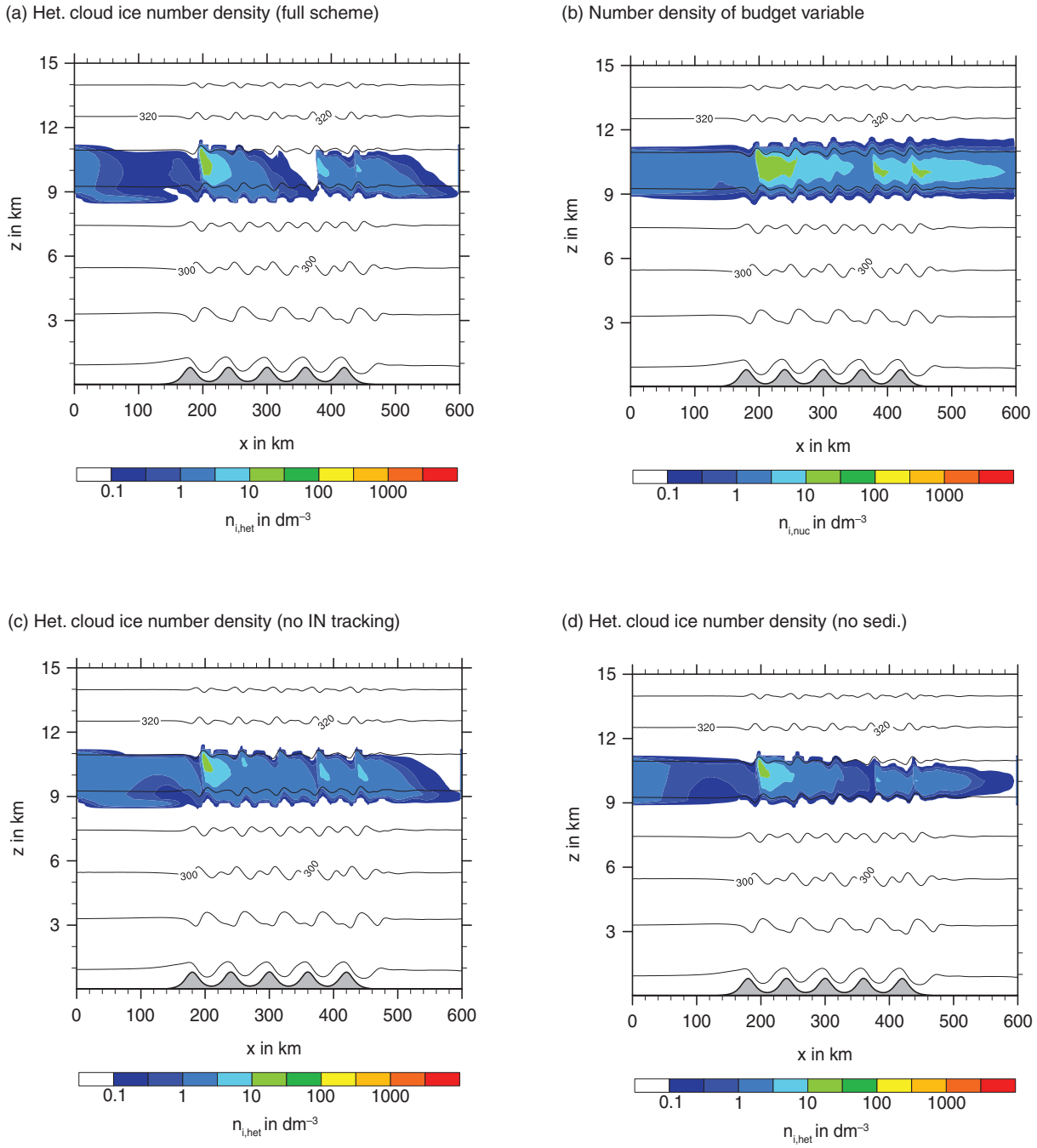

Fig. 9. Idealised simulations of cirrus cloud developed by heterogeneous freezing after 12 hours. The ideal setup consists of the mountain height $h_{max} = 0.8$ km, the horizontal velocity $u_0 = 12$ m s^{-1}, the ice supersaturated layer with $RH_i = 130\%$ and the factor $\chi_{IN} = 3$ for the aerosol distribution. The heterogeneously formed cloud ice with cloud ice sedimentation and the limitation of the activated ice nuclei (IN) tracking is shown in (a). The number density for activated IN $n_{i,nuc}$ is shown in (b). Simulations without IN tracking and without sedimentation are depicted in (c) and (d), respectively.

than in Fig. 9a. Omitting the IN tracking yields a more stratus-like homogeneous cirrus cloud structure, apart from the first peak, which amounts to $n_{i,het} \approx 10$ dm^{-3}. Another aspect is the vertical extent of the orographic cirrus cloud, which are broader in Fig. 9a and b than in Fig. 9d, which does not include sedimentation. When the terminal fall velocity of cloud ice crystals is neglected, the cirrus cloud is restricted to the region of the initial ice

supersaturation layer. However, the heterogeneous ice crystal number density in Fig. 9d shows the same variability as in Fig. 9a using the tracking variable. In all plots the same overall structure can be seen. The stratiform cirrus results from the high amount of ice supersaturation available. The primary gravity wave then serves as an additional trigger for the origin of the ice crystal number density maximum at $x = 200$ km with $n_{i,het} = 50\ dm^{-3}$. The horizontal wind causes the ice crystals to be advected downstream. A second maximum, a magnitude smaller than the first, is then visible over the last hill near $x = 400$ km and the ice crystal number density decreases to the right. Thus, the tracking of activated IN reorganises the inner cloud ice crystal distribution, while cloud ice sedimentation changes the vertical structure. In summary, the introduction of the IN tracking, as well as the cloud ice sedimentation process, significantly alters the spatial structure of cirrus clouds. Consequently these changes in the ice nucleation scheme of the model have a strong impact on the interrelation of heterogeneous and homogeneous nucleation.

In the following, a parameter study is performed to investigate the sensitivity of the two nucleation mechanisms with respect to the initial aerosol number density and mountain height. The impact of the sedimentation and budget variable on the varying degree of dominance of the ice modes is of particular interest. The aerosol scaling factor χ_{IN} ranging from 0.01 to 10 is multiplied to the total of IN, that is, the dust, soot and organic quantities. A value of $\chi_{IN} = 1$ represents the IN amount as suggested in Phillips et al. (2008). The maximum mountain height h_{max} for the five hills ranges between 0.5 and 1.5 km for the parameter study. For the parameter space plots in Fig. 10, the idealised simulations are sampled over 12 hours regarding the amount of homogeneous cloud ice mixing ratio over the total amount of cloud ice, that is, $q_{i,hom}/(q_{i,hom} + q_{i,het})$. The focus lies on the effect that the introduction of the IN tracking variable and cloud ice sedimentation have on the competition between homogeneous and heterogeneous nucleation. Figure 10a includes all cloud ice model changes. In Fig. 10b the budget variable is not accounted for, whereas in Fig. 10c cloud ice particle sedimentation is not included. Figure 10d neglects the autoconversion of cloud ice to snow. The emphasis lies on the diagonal starting at the bottom left corner and ending at the upper right corner. This marks the transition area between the dominant homogeneous freezing for large orographic forcing and low available IN (upper left hand corner) and the heterogeneous nucleation dominated regime for lower mountain heights and higher IN number concentrations (lower right hand corner).

Comparing the full cloud ice scheme in Fig. 10a–c, where the IN budget variable and cloud ice sedimentation are neglected, shows that the two regimes are most clearly separated when using the full scheme (Fig. 10a). Not accounting for these two changes in the cloud ice scheme leads to an increase in the heterogeneous cloud ice mixing ratio and even influences scenarios with high mountain heights and low IN number concentration. Homogeneous freezing dominated regimes are then displaced and only exist for mountain heights above 1000 m when there are hardly any IN available. When only neglecting the budget variable, the competitive behaviour shown in Fig. 10c still looks very similar to plot Fig. 10b for strong orographic forcings. The budget variable has the highest impact for high IN numbers, while the sedimentation has a higher impact on low IN number densities. Omitting cloud ice sedimentation modifies the intermediate regimes and extends the transition between the two nucleation mechanisms, as the larger, heterogeneously nucleated ice particles remain in the orographically induced cirrus cloud and consequently decrease the mass ratio $q_{i,hom}/(q_{i,hom} + q_{i,het})$. Thus, the parameter study stresses the importance of including these processes in order to achieve a more physical representation of the homogeneous and heterogeneous regimes and their competition.

In Fig. 10d, the parameterisation for the autoconversion of cloud ice to snow due to cloud ice crystal aggregation S_{au} is neglected. Otherwise S_{au} is

$$S_{au} = \max(c_{i,au}(q_i - q_{i,0}), 0) \tag{44}$$

in the operational setup with the coefficient $c_{i,au} = 10^{-3}\ s^{-1}$ for cloud ice and the autoconversion threshold $q_{i,0} = 0$ (Doms et al., 2007). Figure 10d shows a clear increase in the dominance of heterogeneous nucleation, even for very low IN. This result indicates that primarily the larger, heterogeneously nucleated ice crystals are transformed into snow through autoconversion. Whereas the explanation sounds plausible, it is astonishing how much impact the individual source and sink terms have and how important it is to account for them diligently. The idealised simulations lead to the conclusion that, on a small scale, homogeneous nucleation is a very important process. They clearly outline its substantial dependency on the vertical velocity as a trigger. Heterogeneous nucleation, on the other hand, is strongly sensitive to the tracking of previously activated IN. Cloud ice sedimentation alters the cirrus cloud structure, enhancing the dominance of smaller, homogeneously nucleated ice crystals, as they do not fall out as quickly as larger, heterogeneously nucleated ice particles. The idealised simulations highlight the different cloud ice properties of homogeneously and heterogeneously nucleated ice. Thus, it is of importance to include both nucleation mechanisms, along with the performed cloud ice scheme improvements in

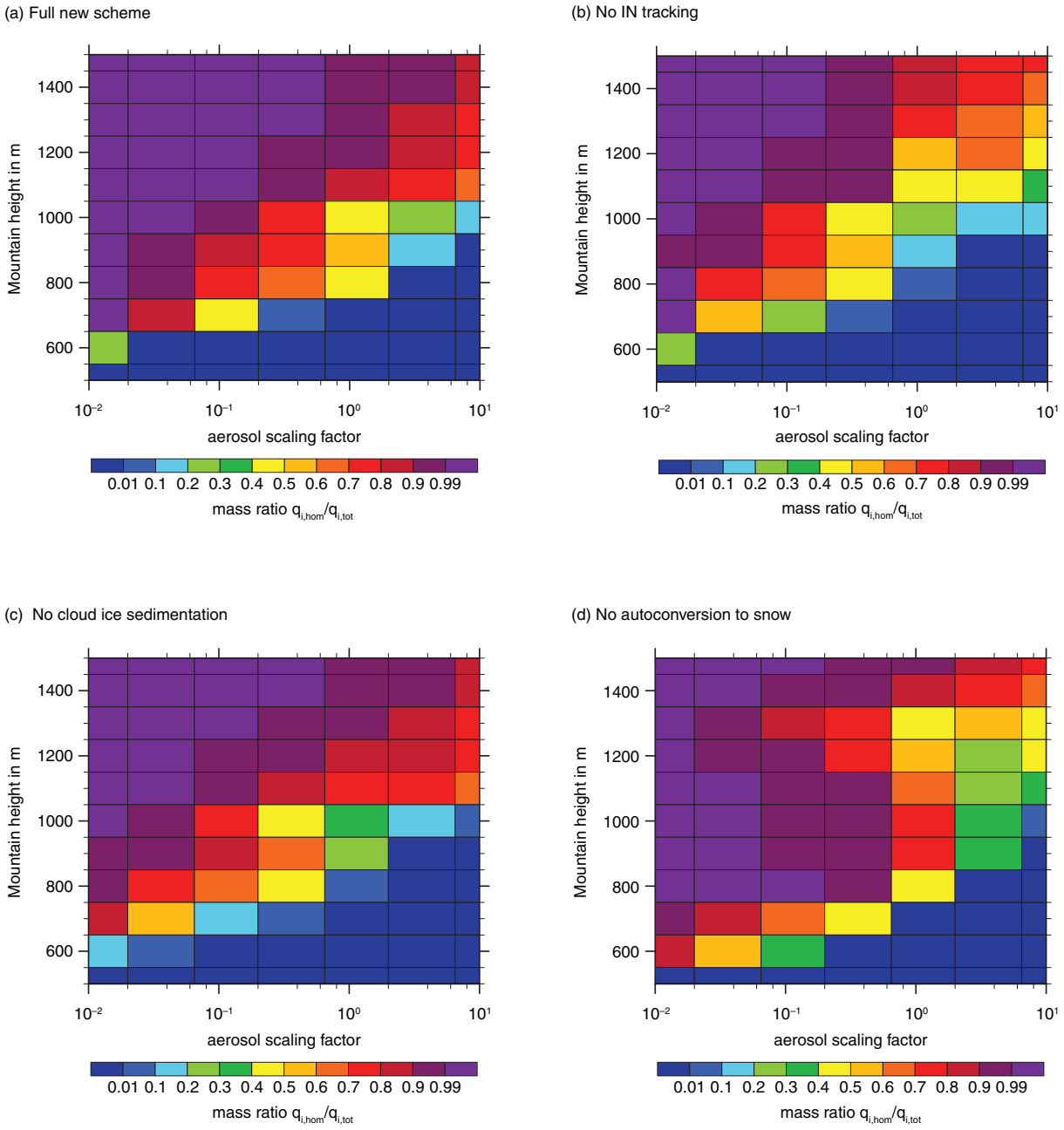

Fig. 10. Parameter space plot showing the dependency of homogeneous and heterogeneous freezing on orographic forcing and aerosol number concentration. (a) shows the results with sedimentation and IN tracking, (b) without the same without the latter. (c) is without ice cloud sedimentation and (d) only excludes the autoconversion of cloud ice to snow.

the NWP model, in order to more realistically describe the behaviour of cirrus clouds.

5. Summary and conclusion

Cirrus clouds are one of the least understood cloud types with a strong impact on climate (Barahona and Nenes, 2008). We have presented a hierarchy of models to simulate and disentangle the processes which are involved in the formation, growth and dissipation of cirrus clouds. The vertical velocity and the presence of IN are known to be the most important factors for cirrus cloud formation as, for example, stated by Haag and Kärcher (2004).

Our study elucidates the complex interaction of the mechanisms dominating homogeneous and heterogeneous nucleation. For this purpose a two-moment two-mode

cloud ice nucleation scheme was developed and tested in a parcel model and idealised COSMO model environment. In the new cloud ice scheme the depositional growth, the cloud ice sedimentation and the fluctuations in the vertical velocity are accounted for, in addition to two new prognostic variables, namely the ice crystal number concentration and the budget variable for activated IN. This scheme was used to examine the mentioned dependencies and atmospheric processes in detail. The resulting new cloud ice scheme is an extension of the operational ice-microphysical parameterisation in the NWP models at the German Weather Service (DWD). In particular, the operational ice microphysics scheme lacks the representation of homogeneous nucleation of liquid aerosol droplets and cloud ice sedimentation. Furthermore, the cloud ice crystal number from the operational cloud ice scheme only includes an empirical parameterisation that describes the increasing number of IN or ice crystals with decreasing temperature, and does not distinguish between different nucleation modes. Though ice supersaturation is permitted as depositional growth is explicitly resolved, as soon as cloud ice is formed it rapidly depletes any existing supersaturation. A limiter is required to prevent more water vapour from being depleted than is available. These deficiencies of the operational ice microphysics scheme make a more physical approach for ice nucleation and ice supersaturation very attractive.

The new cirrus scheme is compatible with both the non-hydrostatic regional model COSMO and the global model GME, which uses a coarser grid and longer timestep. The new scheme ensures numerical stability as well as physical consistency for a wide range of scales. Ice nucleation is described using state-of-the-art parameterisations for homogeneous and heterogeneous nucleation, although heterogeneous nucleation remains a major uncertainty. While the latter mainly depends on the existence of IN, homogeneous freezing of supercooled liquid aerosol occurs in regions with high ice supersaturations and high cooling rates, that is, in strong vertical updrafts. Further extensions to the operational scheme were made, such as particle sedimentation and tracking for activated IN, which is necessary to avoid an overestimation of heterogeneously nucleated ice particles. A relaxation time scale method is applied to achieve a consistent treatment of the depositional growth of the two small-particle ice modes and the larger snowflakes.

An important feature of the microphysics scheme of the DWD models is that the depositional growth process is explicitly modelled. This is not the case in many other, especially global models (e.g. ECMWF's IFS model), which assume in-cloud saturation and consequently convert all humidity exceeding saturation to ice once nucleation is triggered (Tompkins et al., 2007). However in the COSMO and GME, in-cloud supersaturation is explicitly allowed and in the revised scheme the depletion of supersaturation is physically represented with a relaxation timescale. Such an approach is consistent with observations as, for example, Ovarlez et al. (2002) and Comstock et al. (2004) show in-cloud ice supersaturation to be a common phenomenon. Using 1 year of Raman lidar measurements in 2000 at the Southern Great Plains facility near Lamont, Oklahoma, Comstock et al. (2004) finds that $RH_i > 100\%$ is found in about 31% of the cloudy data points. Khvorostyanov and Sassen (2002) also point out that there is a residual ice supersaturation of 5–10% a few hours after a cloud has developed. Idealised COSMO model simulations of orographic cirrus were performed in order to better understand the sensitivities concerning the existence of IN and strong vertical updrafts. Opposed to previous studies with a simpler single mountain setup, for example, by Joos et al. (2009, 2014), we consider a more complex gravity wave setup. This systematic sensitivity study showed that the number of available IN and the detailed choices in the design of the scheme do matter for the competition of heterogeneous versus homogeneous nucleation. Especially the transitional regime, in which both nucleation modes are present, depends strongly on the choice of parameterised processes, second-order processes like IN tracking, and the details of the growth and conversion processes. This sensitivity was demonstrated for the autoconversion of cloud ice to snow, where omitting this term would cause a clear dominance of heterogeneously nucleated ice.

The delicate sensitivity of cirrus clouds to the number of IN available for heterogeneous nucleation does of course ask for a prognostic treatment of aerosols and, eventually, atmospheric chemistry, for example, by using a framework like COSMO-ART (Vogel et al., 2009). For operational NWP this may only be feasible using a hierarchy of models at different grid spacing, that is, predicting aerosols and chemistry only on the large scale, for example, using the MACC system (Bellouin et al., 2013) as an input for high-resolution models that carry only a simplified treatment of the atmospheric aerosol.

The high uncertainty which comes with such delicate sensitivities also highlights the need for reliable observations of the microphysical properties of cirrus clouds. Because of the limitations of our understanding of, for example, heterogeneous ice nucleation and the strong non-linear feedbacks which occur due to the competition of heterogeneous and homogeneous nucleation, a sound empirical basis is crucial for further advancing model development and our understanding of cirrus clouds.

6. Acknowledgements

We would like to thank the two anonymous reviewers, Vivek Sant and Daniel Lee for providing valuable comments on

the draft version. We would also like to thank Bernd Kärcher, Klaus Gierens, Peter Spichtinger and Vaughan Phillips for fruitful discussions. Ulrich Schumann and George Craig are also gratefully acknowledged for their support and interest in this work. This research contributed to the Klimazwei project 'Environmentally Compatible Flight Route Optimization' supported by the DFG. Parts of this research (A.S.) were carried out as part of the Hans Ertel Centre for Weather Research. This research network of universities, research institutes and the Deutscher Wetterdienst is funded by the BMVI (Federal Ministry of Transport, Building and Urban Development).

7. Appendix

A. Overview of the applied parameterisations

In this appendix, a short introduction to the parameterisations which are used in this work is given. These parameterisations include the homogeneous nucleation parameterisations from Kärcher et al. (2006) and Koop et al. (2000), as well as the heterogeneous nucleation scheme by Phillips et al. (2008). Moreover, the relevant equations for the cloud ice sedimentation based on Khvorostyanov and Curry (2005) are shown.

A.1. Heterogeneous nucleation

The Phillips et al. (2008) scheme for heterogeneous nucleation accounts for the model temperature, pressure, water vapour mixing ratio and supersaturation ratio. The number concentration of active IN from the IN species X (i.e. DM, BC and O) within a size interval d log D_X as described in detail in PDA08 is

$$n_{\mathrm{IN,X}} = \int_{\log[D_{\min}]}^{\infty} (1 - \exp[\mu_X\ (D_X, S_i, T)]) \frac{\mathrm{d}n_X}{\mathrm{d}\log D_X} \mathrm{d}\log D_X, \tag{45}$$

which is valid for $T < 0^\circ$C and $1 < S_i \leq S_{i,w}$ where $S_{i,w}$ is the value for water saturation. The function μ_X comprises various relations for the modes and surface area, giving the average number of activated embryos per insoluble aerosol particle with the size D_x. Larger particles have a higher nucleation efficiency due to more effective and active sites. The assumed minimum diameter for an IN is $D_{\min} = 0.1$ μm.

The frozen IN fractions $n_{\mathrm{frac,X}}$ of the individual groups are calculated by dividing the nucleated ice crystal number concentration through the total initially available number of IN for each IN species $\mathrm{IN_X}$. The total heterogeneously nucleated number density $n_{\mathrm{i,het}}$ is then calculated by computing the sum over the three aerosol species.

$$n_{\mathrm{i,het}} = \sum_{X=1}^{3} \mathrm{IN_X}\ n_{\mathrm{frac,X}}. \tag{46}$$

A.2. Homogeneous nucleation

In this work, two different homogeneous nucleation schemes are used, namely by Koop et al. (2000) and Kärcher et al. (2006). These are briefly introduced in the following.

A.2.I. Scheme by Koop et al. (2000)

The classical nucleation theory approach uses an explicit nucleation rate J, often given in units of $\mathrm{cm^{-3}s^{-1}}$. A diagnostic formulation of J describing the freezing rate of supercooled aerosol particles per unit time and per unit volume of aerosol is proposed in Koop et al. (2000). The nucleation rate is of special interest for solving the analytical equation for the change in number density n_i for homogeneous nucleation:

$$\frac{dn_i}{dt} = n_0 J V_0 \quad \text{with} \quad V_0 = \frac{4\pi r_0^3}{3}. \tag{47}$$

The initial volume V_0 with the typical freezing aerosol radius is $r_0 = 0.25$ μm and the aerosol number density prior to freezing n_0, where realistic values are 100–300 $\mathrm{cm^{-3}}$ (Minikin et al., 2003; Spichtinger and Gierens, 2009a). In order to calculate the nucleation rate it has to be noted that the relative humidity RH is assumed to be equal to the water activity a_w when pure liquid bulk water is in equilibrium to water vapour. The water activity a_w is the ratio of the vapour pressure of the solution to the water pressure of pure water at the same temperature. Thus a_w gives the temperature-, concentration- and pressure-dependent water activity of a solution, in this case H_2SO_4, and a_w^i (T, p) of ice. Following Koop et al. (2000), the nucleation rate is then calculated by

$$\log(J) = -906.7 + 8502\Delta a_w - 26924(\Delta a_w)^2 + 29180(\Delta a_w)^3 \tag{48}$$

with $\Delta a_w = a_w - a_w^i$. This is implemented in the parcel model introduced in Section 2. Homogeneous nucleation is triggered at pressures below 350 hPa and temperatures approximately below 235 K (Kärcher and Lohmann, 2002), thus the values are chosen accordingly. Exemplarily, the critical nucleation rate for $S_{i,cr}$, $J_{cr} = 3(4\pi r_0^3 \Delta t)^{-1}$, results in $J_{cr} \approx 10^{10}$ $\mathrm{cm^{-3}\ s^{-1}}$ for the typical time step for general circulation models (GCM) of $\Delta t = 20$ min (Kärcher and Lohmann, 2002). In Table 7.2. in Pruppacher and Klett (1997) this approximated nucleation rate J_{cr} is reached for a supercooling of about 39°C, which agrees well with the Koop et al. (2000) results. As Jensen and Toon (1994) state,

the nucleated ice crystal number is insensitive to the number of available aqueous aerosols, as the competition for water vapour causes the event to cease.

A.2.II. Scheme by Kärcher et al. (2006)

The KHL06 parameterisation for homogeneous nucleation takes the competition between the two nucleation processes into account. This is done by using a fictitious vertical velocity w_p which accounts for pre-existing ice particles

$$w_p = \frac{a_2 + a_3 S_i}{a_1 S_i} R_i, \quad w_p \geq 0 \tag{49}$$

with

$$a_1 = \frac{L_s M_w\, g}{c_p\, RT^2} - \frac{Mg}{RT}, \quad a_2 = \frac{1}{n_{sat}} \quad \text{and} \quad a_3 = \frac{L_s^2 M_w m_w}{c_p\, pT\, M}. \tag{50}$$

The parameters needed in the following are latent heat of sublimation $L_s = 2.836 \times 10^6$ J kg^{-1}, molecular mass of water $M_w = 18 \times 10^{-3}$ kg mol^{-1}, universal gas constant $R = 8.314$ J mol^{-1} K^{-1}, molecular mass of air $M = 29 \times 10^{-3}$ kg mol^{-1} and the mass of a water molecule $m_w = 3 \times 10^{-26}$ kg. The term $n_{sat} = e_{si}/(k_b\, T)$ denotes the number density at saturation per unit volume, where $k_b = 1.38065 \times 10^{-23}$ J K^{-1} is the Boltzmann constant. As lower velocities cause lower ice supersaturations, reducing the velocity has the same effect as nucleated crystals, reducing the saturation due to depositional growth. The freezing or growth term used in eq. (49) is given by

$$R_i = \frac{4\pi}{\nu} n_i r_i^2 \frac{dr_i}{dt}, \tag{51}$$

where $\nu = 3.234 \times 10^{-29}$ m^{-3} denotes the specific volume of a water molecule with respect to ice and the depositional growth $\dot{r}_i$ as defined in the kinetic equation used by Kärcher and Lohmann (2002, KL02 hereafter).

The sensitivity of the cloud ice number density n_i towards w is shown in KL02 where the following relation is derived:

$$n_i \propto w^{3/2} n_{sat}^{-1/2}. \tag{52}$$

This supports the approach of accounting for pre-existing ice through the artificial downdraft term w_p. It depends on the vertical velocity and the particle size conditions:

$$\delta = b_2 r_0, \quad \kappa = \frac{2 b_1 b_2}{1+\delta} \tau_{freez}. \tag{53}$$

The terms b_1 and b_2 are from the equation for the change in crystal size $\dot{r}_i$ given by eq. (60) and are based on KL02.

The dependence of the ice crystal numbers on the vertical velocity is also visible in the equation for the ice crystal number density from the KHL06 parameterisation

$$n_{i,hom} = \frac{a_1 S_i}{a_2 + a_3 S_i} (w - w_p) R_{im}^{-1}, \tag{54}$$

where

$$R_{im} = \frac{4\pi}{\nu} \frac{b1}{b_2^2} \frac{\delta^2}{1+\delta} \left[1 - \frac{1}{\delta^2} + \frac{1}{\delta^2} \left(\frac{(1+\delta)^2}{2} + \frac{1}{\kappa} \right) f(\kappa) \right] \tag{55}$$

is the freezing or growth integral analytically solved for a given initial radius r_0. The analytical estimate of the ice crystal radius at the end of the model time step r_i (Δt), as given in KL02, is used to account for the depositional growth immediately after the nucleation event. The terms $b_1 = \nu \alpha_d \nu_{th} n_{sat}(S_i - 1)/4$ and $b_2 = \alpha_d \nu_{th}/(4 D_v C)$ with the thermal speed of water molecules ν_{th}, the diffusion coefficient of water vapour in the air D_v vapour in air as stated in Pruppacher and Klett (1997). The capacitance for spherical particles is $C = 1$ and the deposition coefficient is set to $\alpha_d = 0.5$. The function $f(\kappa)$ is an asymptotic expansion including an analytically derived error function to prohibit divergence when κ is close to 1 (see detailed derivation in Ren and MacKenzie, 2005). In eq. (55), δ is the dimensionless ice particle size parameter and κ is the ratio of time scales of the initial growth and freezing time scale. It is used to distinguish between the slow ($\kappa \ll 1$) and fast ($\kappa \gg 1$) growth regime.

A.3. Cloud ice sedimentation

The cloud ice sedimentation scheme is based on Khvorostyanov and Curry (2005). The terminal velocity is calculated by equating the drag force to the difference between gravitational and buoyancy force. The challenge here lies in determining the Best number

$$X = C_D Re^2 = \frac{2 mg \rho_a D^2}{A \eta^2} \tag{56}$$

with C_D being the drag coefficient, Re the Reynolds number and η the dynamic viscosity.

A physically based power-law like representation for the relation between the Reynolds number Re and the Best number X is given by Mitchell (1996), while Mitchell and Heymsfield (2005) reformulated this in terms of $m - D$ and $A - D$ parameters. A continuous formulation over the entire size range of liquid and crystalline particles is presented by Khvorostyanov and Curry (2005). Additional corrections for the transition of laminar to turbulent flow and change in air density are accounted for. This resulting terminal fall velocity as a function of D as stated in KC05 is

$$v_i^T = A_v D^{B_v}, \tag{57}$$

$$\text{with } A_v = a_{Re}\rho_a^{b_{Re}-1}\eta^{1-2b_{Re}}\left(\frac{2\alpha g}{\gamma}\right)^{b_{Re}}, \tag{58}$$

$$\text{and } B_v = b_{Re}(\beta-\sigma+2)-1. \tag{59}$$

The continuous functions a_{Re} and b_{Re} are determined in terms of the relation $Re(X)=a_{Re}\,X^{b_{Re}}$. They are defined in eqs. (2.7) and (2.8) in Khvorostyanov and Curry (2005). η is the dynamic viscosity. The equivalent diameter described by eq. (40) is used with the exponents for small hexagonal plates $\alpha=0.587$, $\beta=2.45$, $\gamma=0.12$ and $\sigma=1.85$ (Mitchell, 1996).

B. Kinetic and thermodynamic formulation for depositional growth

Different formulations where used in Section 2.4.I for the homogeneous and the heterogeneous nucleated ice crystals. First, the kinetic formulation is considered, which becomes important for particles with radii comparable to the mean free path of air molecules, like those evolving from homogeneous nucleation. The kinetic equation for the change in crystal size $\dot{r}_i$ used in the KHL06 scheme [see eq. (51)] is given by

$$\frac{dr_i}{dt} = \frac{m_w}{\rho_i}\,\frac{\alpha_d\nu_{th}}{4}\,\frac{n_{sat}(S_i-1)}{1+\frac{\alpha_d\nu_{th}r_i}{4D_v}}, \tag{60}$$

where D_v is the diffusion coefficient of water vapour in air, ν_{th} is the mean of the magnitude of the thermal velocity, $m_w=M_w/N_a$ is the mass of a water molecule with N_a being the Avogadro constant. The term $n_{sat}=e_{si}/(k_bT)$ denotes the number density at saturation per unit volume, where k_b is the Boltzmann constant. In eq. (60) the value $\alpha_d=0.5$ is the deposition coefficient of water molecules onto ice particles, which are assumed spherical as proposed by Spichtinger and Gierens (2009a). The mass accommodation coefficient is normally set to one and was neglected in eq. (17).

Substituting n_{sat}, eq. (60) and

$$S_i = \frac{(q_v-q_{v,si})}{q_{v,si}}+1 \tag{61}$$

into eq. (17) results in the kinetic formulation for the change in cloud ice mixing ratio for the homogeneously nucleated ice crystals due to depositional growth

$$\left.\frac{dq_i}{dt}\right|_{dep,hom} = \frac{\pi n_i r_i^2 m_w \alpha_d \nu_{th} e_{si}}{q_{v,si}\rho_a k_b T\left(1+\frac{\alpha_d\nu_{th}r_i}{4D_v}\right)}(q_v-q_{v,si}). \tag{62}$$

The thermodynamic equation is based on Maxwell's diffusion equation (Maxwell, 1890), which was verified by laboratory studies for frozen prolate spheroids with diameters D_i larger than 100 µm (Korolev et al., 2003). Thus the depositional growth of heterogeneous nucleated ice crystals are described by the thermodynamic equation. Maxwell's diffusion equation is based on steady-state assumptions of a spherical ice crystal in an isothermal surrounding. The formulation as given by Khvorostyanov (1995) and Khvorostyanov and Sassen (1998b) reads:

$$\frac{dr_i}{dt} = \frac{D_v\rho_a C}{\rho_i Q_i r_i \xi_i^2}(q_v-q_{v,si}), \tag{63}$$

in which C represents the capacitance and ξ_i the characteristic dimension of crystals. The term $Q_i=1+(L_s/c_p)(\partial q_{v,si}/\partial T)$ accounts for psychrometric corrections. When assuming spherical particles $C=\xi_i=1$ and $Q_i\approx 1$. Inserting eq. (63) into eq. (17) yields the change in cloud ice mixing ratio

$$\left.\frac{dq_i}{dt}\right|_{dep,het} = \frac{4\pi}{\rho_a}\rho_i n_i r_i^2 \frac{D_v\rho_a C}{\rho_i Q_i r_i \xi_i^2}(q_v-q_{v,si}) \tag{64}$$

$$= 4\pi D_v r_i n_i (q_v-q_{v,si}). \tag{65}$$

The thermodynamically formulated depositional rate used in the operational models of the DWD assume the ice crystals are hexagonal. Thus the form factor for hexagonal plates $a_{i,m}=130$ kg m^{-3} is included and the diameter D_i is defined through the ice crystal mass $m_i=a_{i,m}D_i^3$. The diameter D_i is restricted to 200 µm in the models. H_i is the Howell factor (Howell, 1949) which incorporates effects arising from the difference in the ambient air and the drop temperature, and thus thermal diffusivity

$$\left.\frac{dq_i}{dt}\right|_{dep,het} = \frac{4\pi D_v D_i n_i}{1+H_i}(q_v-q_{v,si}) \tag{66}$$

where

$$H_i = \frac{D_v L_s^2}{K_T R_v T^2}\rho_a q_{v,si}. \tag{67}$$

Without accounting for H_i, eqs. (65) and (66) are equivalent. Equation (66) is used for the depositional growth of the heterogeneously nucleated ice crystals in the following.

As it is of interest how the kinetic equation is related to the thermodynamic formulation, the rate of change in radius eq. (60) is converted into eq. (63). The key difference between both equations lies in the factor

$$1+\frac{\alpha_d\nu_{th}r_i}{4D_v} \sim \frac{\alpha_d\nu_{th}r_i}{4D_v}, \quad \text{for} \quad \frac{\alpha_d\nu_{th}r_i}{4D_v} \gg 1 \tag{68}$$

which holds for $r_i \gg r_{i,0}$. The detailed formulation reads

$$\frac{\alpha_d\nu_{th}r_i}{4D_v} = \frac{1}{8}\sqrt{\frac{8k_bT}{\pi m_w}}r_i\left(2.11\times10^{-5}\left(\frac{T}{T_0}\right)^{1.94}\left(\frac{p_0}{p}\right)\right)^{-1} \tag{69}$$

for $\alpha_d=0.5$. Starting out with the kinetic formulation and assuming the ice crystal radii $r_i \gg r_{i,0}$, the kinetic approach can be reformulated by applying the simplification from eq. (68).

Subsequently, eq. (61) and n_{sat} are inserted into eq. (60) which yields

$$\frac{dr_{\mathrm{i}}}{dt} = \frac{m_{\mathrm{w}} D_{\mathrm{v}}}{\rho_{\mathrm{i}} r_{\mathrm{i}}} \frac{e_{\mathrm{si}}}{k_{\mathrm{b}} T} \frac{(q_{\mathrm{v}} - q_{\mathrm{v,si}})}{q_{\mathrm{v,si}}}. \tag{70}$$

With the further substitution of $e_{\mathrm{si}} = R_{\mathrm{v}}/R_{\mathrm{a}} p q_{\mathrm{v,si}}$

$$\frac{dr_{\mathrm{i}}}{dt} = \frac{D_{\mathrm{v}} \rho_{\mathrm{a}}}{\rho_{\mathrm{i}} r_{\mathrm{i}}} (q_{\mathrm{v}} - q_{\mathrm{v,si}}) \tag{71}$$

is obtained, that is, the thermodynamic equation eq. (63) for spherical particles.

References

Andrejczuk, M., Grabowski, W. W., Malinowski, S. P. and Smolarkiewicz, P. 2009. Numerical simulation of cloud–clear air interfacial mixing: homogeneous versus inhomogeneous mixing. *J. Atmos. Sci.* **66**, 2493–2500. DOI: 10.1175/2009JAS2956.1.

Baldauf, M., Seifert, A., Förstner, J., Majewski, D., Raschendorfer, M. and co-authors. 2011. Operational convective-scale numerical weather prediction with the COSMO model: description and sensitivities. *Mon. Weather Rev.* **139**, 3887–3905. DOI: 10.1175/MWR-D-10-05013.1.

Barahona, D. and Nenes, A. 2008. Parameterization of cirrus cloud formation in large-scale models: homogeneous nucleation. *J. Geophys. Res.* **113**(D11), D11211. DOI: 10.1029/2007JD009355.

Barahona, D. and Nenes, A. 2009. Parameterizing the competition between homogeneous and heterogeneous freezing in cirrus cloud formation-monodisperse ice nuclei. *Atmos. Chem. Phys.* **9**, 369–381. DOI: 10.5194/acp-9-369-2009.

Baumgardner, D., Avallone, L., Bansemer, A., Borrmann, S., Brown, P. and co-authors. 2012. In situ, airborne instrumentation-addressing and solving measurement problems in ice clouds. *Bull. Am. Meteorol. Soc.* **93**, E29–E34. DOI: 10.1175/BAMS-D-11-00123.1.

Bellouin, N., Quaas, J., Morcette, J.-J. and Boucher, O. 2013. Estimates of aerosol radiative forcing from the MACC re-analysis. *Atmos. Chem. Phys.* **13**, 2045–2062. DOI: 10.5194/acp-13-2045-2013.

Boucher, O., Randall, D., Artaxo, P., Bretherton, C., Feingold, G. and co-authors. 2013. Clouds and Aerosols. In: *Climate Change 2013: The Physical Science Basis. Contribution of Working Group I to the Fifth Assessment Report of the Intergovernmental Panel on Climate Change* (eds. T.F. Stocker, D. Qin, G.- K. Plattner, M. Tignor and S.K. Allen) Cambridge University Press, Cambridge, UK, NY, USA, pp. 571–658. DOI: 10.1017/CBO9781107415324.016.

Burkhardt, U. and Kärcher, B. 2011. Global radiative forcing from contrail cirrus. *Nat. Clim. Change.* **1**, 54–58. DOI: 10.1038/NCLIMATE1068.

Cohard, J. M. and Pinty, J. P. 2000. A comprehensive two-moment warm microphysical bulk scheme. I: description and tests. *Q. J. Roy. Meteorol. Soc.* **126**, 1815–1842.

Comstock, J. M., Ackermann, T. P. and Turner, D. D. 2004. Evidence of high ice supersaturation in cirrus clouds using ARM Raman lidar measurements. *Geophys. Res. Lett.* **31**(11), L11106. DOI: 10.1029/2004GL019705.

Czizco, D., Froyd, K., Hoose, C., Jensen, E., Diao, M. and co-authors. 2013. Clarifying the dominant sources and mechanisms of cirrus cloud formation. *Science.* **340**, 1320–1324. DOI: 10.1126/science.1234145.

DeMott, P. J., Meyers, M. P. and Cotton, W. R. 1994. Parameterization and impact of ice initiation processes relevant to numerical model simulations of cirrus clouds. *J. Atmos. Sci.* **51**, 77–90.

DeMott, P. J., Möhler, O., Stetzer, O., Vali, G., Levin, Z. and co-authors. 2011. Resurgence in ice nuclei measurement research. *Bull. Am. Met. Soc.* **102**, 1623–1635. DOI: 10.1175/2011BAMS3119.1.

DeMott, P. J., Rogers, D. C. and Kreidenweis, S. M. 1997. The susceptibility of ice formation in upper tropospheric clouds to insoluble aerosol components. *J. Geophys. Res.* **102**(D16), 19575–19584. DOI: 10.1029/97JD01138.

Doms, G., Förstner, J., Heise, E., Herzog, H.-J., Raschendorfer, M. and co-authors. 2007. *A Description of the Nonhydrostatic Regional Model LM, Part II: Physical Parameterization*. Deutscher Wetterdienst, Offenbach, Germany.

Doms, G., Majewski, D., Müller, A. and Ritter, B. 2004. *Recent Changes to the Cloud-Ice Scheme*. COSMO Newsletter No. 4. Online at: http://www.cosmo-model.org/content/model/documentation/newsLetters/newsLetter04/chp9-8.pdf

Eidhammer, T., DeMott, P. J. and Kreidenweis, S. M. 2009. A comparison of heterogeneous ice nucleation parameterizations using a parcel model framework. *J. Geophys. Res.* **114**, D06202. DOI: 10.1029/2008JD011095.

Field, P., Hogan, R., Brown, P., Illingworth, A., Choularton, T. and co-authors. 2005. Parametrization of ice-particle size distributions for mid-latitude stratiform cloud. *Q. J. Roy. Meteorol. Soc.* **131**, 1997–2017.

Fletcher, N. H. 1962. *Physics of Rain Clouds*. Cambridge University Press, Cambridge, UK.

Fukuta, N. and Walter, L. A. 1970. Kinetics of hydrometeor growth from a vapor-spherical model. *J. Atmos. Sci.* **27**, 1160–1172.

Gettelman, A., Liu, X., Ghan, S. J., Morrison, H., Park, S. and co-authors. 2010. Global simulations of ice nucleation and ice supersaturation with an improved cloud scheme in the Community Atmosphere Model. *J. Geophys. Res.* **115**, D18216. DOI: 10.1029/2009JD013797.

Gierens, K. M. 2003. On the transition between heterogeneous and homogeneous freezing. *Atmos. Chem. Phys.* **3**, 437–446.

Gierens, K. M., Monier, M. and Gayet, J.-F. 2003. The deposition coefficient and its role for cirrus clouds. *J. Geophys. Res.* **108**, D2. DOI: 10.1029/2001JD001558.

Haag, W. and Kärcher, B. 2004. The impact of aerosols and gravity waves on cirrus clouds at midlatitudes. *J. Geophys. Res.* **109**, D12202. DOI: 10.1029/2004JD004579.

Haag, W., Kärcher, B., Schäfer, S., Stetzer, O., Möhler, O. and co-authors. 2003. Numerical simulations of homogeneous freezing processes in the aerosol chamber AIDA. *Atmos. Chem. Phys.* **3**, 195–210.

Harrington, J. Y., Lamb, D. and Carver, R. 2009. Parameterization of surface kinetic effects for bulk microphysical models: influences on simulated cirrus dynamics and structure. *J. Geophys. Res.* **114**, D06212. DOI: 10.1029/2008JD011050.

Heymsfield, A., Baumgardner, D., DeMott, P., Forster, P., Gierens, K. and co-authors. 2010. Contrail microphysics. *Bull. Am. Met. Soc.* **91**, 465–472. DOI: 10.1175/2009BAMS2839.1.

Heymsfield, A. J. and Iaquinta, J. 2000. Cirrus crystal terminal velocities. *J. Atmos. Sci.* **57**, 916–938.

Heymsfield, A. J. and Sabin, R. M. 1989. Cirrus crystal nucleation by homogeneous freezing of solution droplets. *J. Atmos. Sci.* **46**, 2252–2264.

Hobbs, P. V. and Rangno, A. L. 1985. Ice particle concentrations in clouds. *J. Atmos. Sci.* **42**, 2523–2548.

Hoose, C., Kristjánsson, J. E., Chen, J.-P. and Hazra, A. 2010. A classical-theory-based parameterization of heterogeneous ice nucleation by mineral dust, soot, and biological particles in a global climate model. *J. Atmos. Sci.* **67**, 2483–2503.

Howell, W. E. 1949. The growth of cloud drops in uniformly cooled air. *J. Meteorol.* **6**, 134–149.

Hoyle, C., Luo, B. and Peter, T. 2005. The origin of high ice crystal number densities in cirrus clouds. *J. Atmos. Sci.* **62**(7), 2568–2579. DOI: 10.1175/JAS3487.1.

Jakob, C. 2002. Ice clouds in numerical weather prediction models-progress, problems and prospects. In: *Cirrus* (eds. D. K. Lynch, K. Sassen, D. O. Starr, and G. Stephens). Oxford University Press, New York, pp. 327–345.

Jensen, E. J., Pfister, L. and Toon, O. B. 2011. Impact of radiative heating, wind shear, temperature variability, and microphysical processes on the structure and evolution of thin cirrus in the tropical tropopause layer. *J. Geophys. Res.* **116**. DOI: 10.1029/2010JD015417.

Jensen, E. J. and Toon, O. B. 1994. Ice nucleation in the upper troposphere: sensitivity to aerosol number density, temperature, and cooling rate. *Geophys. Res. Lett.* **21**, 2019–2022.

Joos, H., Spichtinger, P. and Lohmann, U. 2009. Orographic cirrus in a future climate. *Atmos. Chem. Phys.* **9**, 7825–7845.

Joos, H., Spichtinger, P., Lohmann, U., Gayet, J.-F. and Minkin, A. 2008. Orographic cirrus in the global climate model ECHAM5. *J. Geophys. Res.* **113**, D18205. DOI: 10.1029/2007JD009605.

Joos, H., Spichtinger, P., Reutter, P. and Fusina, F. 2014. Influence of heterogeneous freezing on the microphysical and radiative properties of orographic cirrus clouds. *Atmos. Chem. Phys.* **14**, 6835–6852. DOI: 10.5194/acp-14-6835-2014.

Kärcher, B. and Burkhardt, U. 2008. A cirrus cloud scheme for general circulation models. *Q. J. Roy. Meteorol. Soc.* **134**(635), 1439–1461. DOI: 10.1175/JAS3447.1.

Kärcher, B., Hendricks, J. and Lohmann, U. 2006. Physically based parameterization of cirrus cloud formation for use in global atmospheric models. *J. Geophys. Res.* **111**(D1), D01205. DOI: 10.1029/2005JD006219.

Kärcher, B. and Lohmann, U. 2002. A parameterization of cirrus cloud formation: homogeneous freezing of supercooled aerosols. *J. Geophys. Res.* **107**(D2), 4010. DOI: 10.1029/2001JD000470.

Kärcher, B. and Lohmann, U. 2003. A parameterization of cirrus cloud formation: heterogeneous freezing. *J. Geophys. Res.* **108**(D14), 4402. DOI: 10.1029/2002JD003220.

Kay, J. E., Baker, M. and Hegg, D. 2006. Microphysical and dynamical controls on cirrus cloud optical depth distributions. *J. Geophys. Res.* **111**, D24205. DOI: 10.1029/2005JD006916.

Khvorostyanov, V. 1995. Mesoscale processes of cloud formation, cloud–radiation interaction, and their modelling with explicit cloud microphysics. *Atmos. Res.* **39**, 1–67.

Khvorostyanov, V. I. and Curry, J. A. 2004. The theory of ice nucleation by heterogeneous freezing of deliquescent mixed CCN. Part I: critical radius, energy, and nucleation rate. *J. Atmos. Sci.* **61**, 2676–2691.

Khvorostyanov, V. I. and Curry, J. A. 2005. Fall velocities of hydrometeors in the atmosphere: refinements to a continuous analytical power law. *J. Atmos. Sci.* **62**, 4343–4357.

Khvorostyanov, V. I. and Curry, J. A. 2009. Critical humidities of homogeneous and heterogeneous ice nucleation: inferences from extended classical nucleation theory. *J. Geophys. Res.* **114**, D04207. DOI: 10.1029/2008JD011197.

Khvorostyanov, V. and Sassen, K. 1998a. Cirrus cloud simulation using explicit microphysics and radiation. Part II: microphysics, vapor and ice mass budgets, and optical and radiative properties. *J. Atmos. Sci.* **55**, 1822–1844.

Khvorostyanov, V. and Sassen, K. 1998b. Cirrus cloud simulation using explicit microphysics and radiation. Part I: model description. *J. Atmos. Sci.* **55**, 1808–1821.

Khvorostyanov, V. I. and Sassen, K. 2002. Microphysical processes in cirrus and their impact on radiation. In: *Cirrus* (eds. D. K. Lynch, K. Sassen, D. O. Starr, and G. Stephens). Oxford University Press, New York, pp. 397–432.

Koop, T., Luo, B., Tsias, A. and Peter, T. 2000. Water activity as the determinant for homogeneous ice nucleation in aqueous solutions. *Nature.* **206**, 611–614.

Korolev, A., Bailey, M. P., Hallett, J. and Isaac, G. A. 2003. Laboratory and in situ observation of deposition growth of frozen drops. *J. Appl. Meteorol.* **43**, 612–622.

Korolev, A. and Mazin, I. 2003. Supersaturation of water vapor in clouds. *J. Atmos. Sci.* **60**, 2957–2974.

Krämer, M., Schiller, C., Afchine, A., Bauer, R., Gensch, I. and co-authors. 2009. Ice supersaturations and cirrus cloud crystal numbers. *Atmos. Chem. Phys.* **9**(11), 3505–3522.

Lin, R. F., Starr, D. O., DeMott, P. J., Cotton, R., Sassen, K. and co-authors. 2002. Cirrus parcel model comparison project. Phase 1: the critical components to simulate cirrus initiation explicitly. *J. Atmos. Sci.* **59**, 2305–2329.

Liou, K.-N. 1986. Influence of cirrus clouds on weather and climate processes: a global perspective. *Mon. Weather. Rev.* **114**, 1167–1199.

Liu, X. and Penner, J. E. 2005. Ice nucleation parameterization for global models. *Meteorol. Zeitschr.* **14**, 499–514.

Lohmann, U. and Diehl, K. 2006. Sensitivity studies of the importance of dust ice nuclei for the indirect aerosol effect of stratiform mixed-phase clouds. *J. Atmos. Sci.* **63**, 968–982.

Lohmann, U., Feichter, J., Chuang, C. C. and Penner, J. 1999a. Prediction of the number of cloud droplets in the ECHAM GCM. *J. Geophys. Res.* **104**, 9169–9198.

Lohmann, U., McFarlane, N., Levkov, L., Abdella, K. and Albers, F. 1999b. Comparing different cloud schemes of a single

column model by using mesoscale forcing and nudging technique. *J. Clim.* **12**, 438–461.

Majewski, D., Liermann, D., Prohl, P., Ritter, B., Buchhold, M. and co-authors. 2002. The operational global icosahedral-hexagonal gridpoint model GME: description and high-resolution tests. *J. Atmos. Sci.* **139**, 319–338.

Mannstein, H. 2008. Climate Protection and Adaption-Results of the klimazwei Research Programme-Umweltgerechte Flugroutenoptimierung. Online at: http://www.klimazwei.de/Portals/0/klimazwei-Ergebnisbroschüre.pdf

Maxwell, J. C. 1890. *The Scientific Papers of James Clerk Maxwell.* Cambridge University Press, New York.

Mellor, G. L. and Yamada, T. 1974. A hierarchy of turbulence closure models for planetary boundary layers. *J. Atmos. Sci.* **31**, 1791–1806.

Meyers, M. P., DeMott, P. J. and Cotton, W. R. 1992. New primary ice-nucleation parameterizations in an explicit cloud model. *J. Appl. Meteorol.* **31**, 708–721.

Minikin, A., Petzold, A., Ström, J., Krejci, R., Seifert, M. and co-authors. 2003. Aircraft observations of the upper tropospheric fine particle aerosol in the Northern and Southern Hemisphere at midlatitudes. *Geophys. Res. Lett.* **30**, Nr. 10, 1503. DOI: 10.1029/2002GL016458.

Mironov, D. V. 2009. Turbulence in the lower troposphere: second-order closure and Mass-Flux modelling frameworks. In *Interdisciplinary Aspects of Turbulence* (eds. W. Hillebrandt and F. Kupka). Springer-Verlag, Berlin, pp. 161–222.

Mitchell, D. L. 1996. Use of mass- and area-dimensional power laws for determining precipitation particle terminal velocities. *J. Atmos. Sci.* **53**, 1710–1723.

Mitchell, D. L. and Heymsfield, A. J. 2005. Refinements in the treatment of ice particle terminal velocities, highlighting aggregates. *J. Atmos. Sci.* **62**, 1637–1644. DOI: 10.1175/JAS3413.1.

Morrison, H., Curry, J. and Khvorostyanov, V. 2005a. A new double-moment microphysics parameterization for application in cloud and climate models. Part I: description. *J. Atmos. Sci.* **62**(6), 1665–1677. DOI: 10.1175/JAS3447.1.

Morrison, H., Shupe, M. D., Pinto, J. O. and Curry, J. A. 2005b. Possible roles of ice nucleation mode and ice nuclei depletion in the extended lifetime of Arctic mixed-phase clouds. *Geophys. Res. Lett.* **32**(18), L18801. DOI: 10.1029/2005GL023614.

Murphy, D. M. and Koop, T. 2005. Review of ice and supercooled water for atmospheric applications. *Q. J. Roy. Meteorol. Soc.* **131**, 1539–1565.

Ovarlez, J., Gayet, J.-F., Gierens, K., Ström, J., Ovarlez, H. and co-authors. 2002. Water vapor measurements inside cirrus clouds in northern and southern hemispheres during INCA. *Geophys. Res. Lett.* **29**, 16, Article Nr. 1813. DOI: 10.1029/2001GL014440.

Phillips, V., Andronache, C., Christner, B., Morris, C., Sands, D. and co-authors. 2009. Potential impacts from biological aerosols on ensembles of continental clouds simulated numerically. *Biogeosciences.* **6**, 987–1014.

Phillips, V., DeMott, P. and Andronache, C. 2008. An empirical parameterization of heterogeneous ice nucleation for multiple chemical species of aerosol. *J. Atmos. Sci.* **65**(9), 2757–2783. DOI: 10.1175/2007JAS2546.1.

Phillips, V. T., DeMott, P. J., Andronache, C., Pratt, K. A., Prather, K. A. and co-authors. 2013. Improvements to an empirical parameterization of heterogeneous ice nucleation and its comparison with observations. *J. Atmos. Sci.* **70**, 378–409. DOI: 10.1175/JAS-D-12-080.1.

Phillips, V. T. J., Pokrovsky, A. and Khain, A. 2007. The influence of time-dependent melting on and precipitation production in maritime and continental storm clouds. *J. Atmos. Sci.* **64**, 338–359.

Pruppacher, H. R. and Klett, J. D. 1997. *Microphysics of Clouds and Precipitation*. Kluwer Academic Publishers, Dordrecht.

Ren, C. and MacKenzie, A. R. 2005. Cirrus parameterization and the role of ice nuclei. *Q. J. Roy. Meteorol. Soc.* **131**, 1585–1605. DOI: 10.1256/qj.04.126.

Sassen, K. and Dodd, G. C. 1988. Homogeneous nucleation rate for highly supercooled cirrus cloud droplets. *J. Atmos. Sci.* **45**(8), 1357–1369.

Schumann, U. 2002. Contrail cirrus. In: *Cirrus* (eds. D. K. Lynch, K. Sassen, D. O. Starr, and G. Stephens). Oxford University Press, New York, pp. 231–255.

Seifert, A. 2008. A Revised Cloud Microphysical Parameterization for COSMO-LME. COSMO Newsletter No. 7. Online at: http://www.cosmo-model.org/content/model/documentation/newsLetters/newsLetter07/cnl7-seifert.pdf

Spichtinger, P. and Cziczo, D. 2010. Impact of heterogeneous ice nuclei on homogeneous freezing events in cirrus clouds. *J. Geophys. Res.* **115**, D14208. DOI: 10.1029/2009JD0112168.

Spichtinger, P. and Gierens, K. 2009a. Modelling of cirrus clouds – part 1a: model description and validation. *Atmos. Chem. Phys.* **9**(2), 685–706.

Spichtinger, P. and Gierens, K. 2009b. Modelling of cirrus clouds – part 2: competition of different nucleation mechanisms. *Atmos. Chem. Phys.* **9**, 2319–2334.

Spichtinger, P., Gierens, K. and Wernli, H. 2005. A case study on the formation and evolution of ice supersaturation in the vicinity of a warm conveyer belt's outflow region. *Atmos. Chem. Phys.* **5**, 973–987. DOI: 10.5194/acp-5-973-2005.

Stevens, B. 2011. Twelve lectures on cloud physics, winter semester 2010–2011. *Max-Planck-Institut für Meteorologie*. Online at: http://www.mpimet.mpg.de/fileadmin/staff/stevensbjorn/teaching/skript-5.pdf

Thompson, G., Rasmussen, R. and Manning, K. 2004. Explicit forecasts of winter precipitation using an improved bulk microphysics scheme. Part I: description and sensitivity analysis. *Mon. Weather Rev.* **132**, 519–542.

Tompkins, A., Gierens, K. and Rädel, G. 2007. Ice supersaturation in the ECMWF Integrated Forecast System. *Q. J. Roy. Meteorol. Soc.* **133**, 53–63.

Vogel, B., Vogel, H., Bäumer, D., Bangert, M., Lundgren, K. and co-authors. 2009. The comprehensive model system COSMO-ART-radiative impact of aerosol on the state of the atmosphere on the regional scale. *Atmos. Chem. Phys.* **9**, 8661–8680.

Wang, M. and Penner, J. 2010. Cirrus clouds in a global climate model with a statistical cirrus cloud scheme. *Atmos. Chem. Phys.* **10**, 5449–5474. DOI: 10.5194/acp-10-5449-2010.

Yun, Y., Penner, J. and Popovicheva, O. 2013. The effects of hygroscopicity on ice nucleation of fossil fuel combustion aerosols in mixed-phase clouds. *Atmos. Chem. Phys.* **13**, 4339–4348. DOI: 10.5194/acp-13-4339-2013.